

1-Sulfonyl-3-amino-1*H*-1,2,4-triazoles as Yellow Fever Virus Inhibitors: Synthesis and Structure–Activity Relationship

Elena Kazakova,[§] Thomas R. Lane,[§] Thane Jones,[§] Ana C. Puhl, Olga Riabova, Vadim Makarov, and Sean Ekins*



Cite This: *ACS Omega* 2023, 8, 42951–42965



Read Online

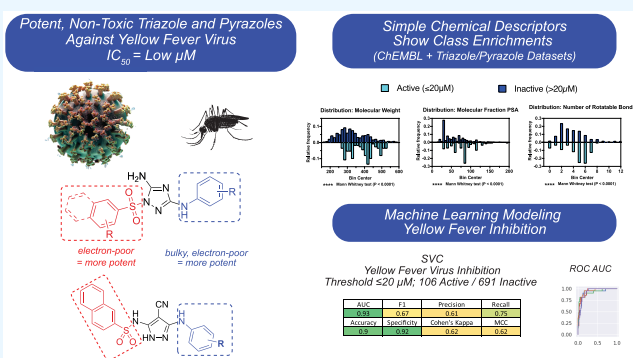
ACCESS |

Metrics & More

Article Recommendations

Supporting Information

ABSTRACT: Yellow fever virus (YFV) transmitted by infected mosquitoes causes an acute viral disease for which there are no approved small-molecule therapeutics. Our recently developed machine learning models for YFV inhibitors led to the selection of a new pyrazolesulfonamide derivative **RCB16003** with acceptable *in vitro* activity. We report that the *N*-phenyl-1-(phenylsulfonyl)-1*H*-1,2,4-triazol-3-amine class, which was recently identified as active non-nucleoside reverse transcriptase inhibitors against HIV-1, can also be repositioned as inhibitors of yellow fever virus replication. As compared to other *Flaviviridae* or *Togaviridae* family viruses tested, both compounds **RCB16003** and **RCB16007** demonstrate selectivity for YFV over related viruses, with only **RCB16007** showing some inhibition of the West Nile virus (EC₅₀ 7.9 μM, CC₅₀ 17 μM, SI 2.2). We also describe the absorption, distribution, metabolism, and excretion (ADME) *in vitro* and pharmacokinetics (PK) for **RCB16007** in mice. This compound had previously been shown to not inhibit hERG, and we now describe that it has good metabolic stability in mouse and human liver microsomes, low levels of CYP inhibition, high protein binding, and no indication of efflux in Caco-2 cells. A single-dose oral PK study in mice has a *T*_{1/2} of 3.4 h and *C*_{max} of 1190 ng/mL, suggesting good availability and stability. We now propose that the *N*-phenyl-1-(phenylsulfonyl)-1*H*-1,2,4-triazol-3-amine class may be prioritized for *in vivo* efficacy testing against YFV.



INTRODUCTION

Yellow fever (YF) is an acute viral hemorrhagic disease transmitted by mosquito-borne flavivirus^{1,2} with the highest prevalence found in Africa and South America³ with mortality rates up to 50%.⁴ Despite the availability of a safe and effective vaccine,⁵ there has been an increase in unvaccinated populations with outbreaks in Brazil and Angola in 2016.^{6–8} This could be due to various reasons, such as vaccine hesitancy, inadequate healthcare infrastructure, and low awareness about the importance of vaccination. At the same time, this opens up the possibility of developing small-molecule drugs. There are currently no approved small-molecule-specific antivirals for the treatment of yellow fever virus infection. Nucleoside analogues, such as ribavirin,⁹ sofosbuvir,¹⁰ galidesivir,¹¹ and favipiravir,¹² have mostly been tested in animal models and have not yet reached clinical trials. Moreover, in recent years, most of the flavivirus drug discovery campaigns have focused on broad-spectrum agents for dengue and Zika viruses, while the need for small-molecule YF inhibitors has not yet been met.¹³

The reason for this lack of attention is the relatively small number of confirmed infections as well as the neglected disease status, which create a limited market size and commercial

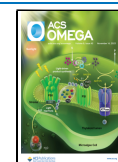
opportunity. Therefore, efforts are still needed to cost-effectively identify new molecules for YFV,¹⁴ such as high-throughput screening (HTS)¹⁵ and machine learning methods.¹⁶ In the simplest form, machine learning approaches use an array of algorithms (e.g., naïve-Bayesian classifier,^{17–19} random forests (rf),^{20,21} or support vector machines (svm))^{22–24} and molecular descriptors (fingerprints or physicochemical properties like log *P* and others) to generate models that can be used to score compound libraries.^{25–27} Rajput and Kumar have previously developed svm and rf regression models with data for many different flaviviruses, although the amount of YFV data used in the training set was comparatively small.²⁸ We have also applied various machine learning approaches to YFV.²⁹ First, we curated YFV cell-based assay data from the literature and public databases and then generated numerous machine learning models. These were

Received: August 17, 2023

Revised: October 10, 2023

Accepted: October 12, 2023

Published: November 1, 2023



validated with an external test set before use for prioritizing and ultimately selecting five compounds for *in vitro* testing. While the training set was limited, one molecule, a pyrazolesulfonamide derivative **RCB16003**, showed a low micromolar potency (EC_{50} 3.2 μ M) and acceptable cytotoxicity (CC_{50} 24 μ M) against YFV and represented a new scaffold suitable for hit-to-lead optimization.²⁹ While sulfonamides are a well-known class of drugs with antiviral activity for HBV,³⁰ HIV,³¹ and HCV,³⁰ they had not previously been described for YFV.

We now describe how we have progressed from **RCB16003** to a similar 1-sulfonyl-3-amino-1*H*-1,2,4-triazole scaffold and describe the structure–activity relationship (SAR) analysis for YFV. We have also characterized **RCB16007** in detail generating absorption, distribution, metabolism, and excretion (ADME) and *in vivo* pharmacokinetics (PK) in mice.

METHODS

Data Curation. The curation of our legacy yellow fever inhibition data was previously described.²⁹ Additional inhibition data were downloaded from ChEMBL (ChEMBL375): ChEMBL ID ChEMBL613731 (yellow fever virus), EC_{50} only. This data was combined with the previously curated data and was then sanitized using our proprietary software “E-Clean”, which uses open-source RD-Kit tools to remove duplicate compounds and salts and neutralize charges. There was significant overlap between these data sets. Prior to combining, each compound was binarized at the model threshold, and only data that had an 80% classification agreement was retained. Based on this, there was some variation in the final data set sizes based on the threshold. Data sets were further standardized within the latest version of the Assay Central software, which uses the Indigo Toolkit.³²

Machine Learning. Machine learning models and algorithms were generated using our proprietary Assay Central software,³³ and this is described further in the [Supporting Information](#). In short, regression and classification models were built from the existing literature using several machine learning algorithms and were validated using 5-fold cross-validation.

t-SNE Visualization. t-SNE³⁴ plots embed data into a lower-dimensional space. For each compound, 1024-bit ECFP6 fingerprints were generated and embedded into a two-dimensional vector using t-SNE. All t-SNE values were generated using the scikit-learn library in python with default hyperparameters ($n_{\text{components}} = 2$, perplexity = 30, early exaggeration = 12.0, learning rate = 200, $n_{\text{iter}} = 1000$).

Synthetic Procedures. General synthesis methods can be found in the [Supporting Information](#). Synthesis of compounds **RCB16007**, **17152**, **17158**, **17159**, **18320**, **20108**, **20116**, **21055**, **21065**, **21066**, and their physicochemical properties were described previously by Lane et al.³⁵

Synthesis of *N'*-Cyano-*N*-Substituted Phenylcarbami-midothioic Acid Methyl Esters **1.** *Method A*.

- (a) Dimethylthiocarbamoyl chloride (1.0–1.1 equiv) was added to a solution of the corresponding aniline (1.0 equiv) in dry toluene or benzene, and the reaction mixture was stirred at reflux for 2–3 h. The mixture was then cooled to room temperature, treated with hexane, and the resulting precipitate was filtered off. The organic solution was evaporated *in vacuo*, and the corresponding isothiocyanatobenzene was obtained and used without further purification.

- (b) A mixture of sodium ethoxide (1.0–1.2 equiv) and cyanamide (1.0 equiv) in ethanol (20 mL) was stirred at room temperature for 30–40 min. The corresponding isothiocyanatobenzene from the previous step (1.0–1.2 equiv) was then added to the mixture. After stirring at room temperature for an additional 1.5 h, iodomethane (2.0–2.5 equiv) was added to the mixture, and the reaction mixture was stirred at reflux for 1–2 h and at room temperature overnight. The resulting precipitate was filtered and dried to give the corresponding phenylcarbami-midothioic acid methyl esters **1**.

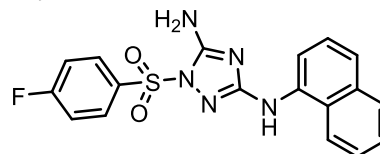
Method B.

- (c) A mixture of the corresponding aniline (1.0–1.2 equiv) and dimethyl cyanodithioiminocarbonate (1.0 equiv) in EtOH (10 mL) was stirred at reflux for 3–4 h. The reaction mixture was then cooled, and the precipitate formed was filtered, washed with hexane, and recrystallized from ethanol to give the corresponding phenylcarbami-midothioic acid methyl esters **1**.

Synthesis of *N*³-Substituted Phenyl-1*H*-1,2,4-triazole-3,5-diamines **2.** A solution of hydrazine hydrate (3.0–5.0 equiv) in water (50 mL) was added to a solution of phenylcarbami-midothioic acid methyl esters **1** (1.0–1.5 equiv) in ethanol (30 mL), and the reaction mixture was stirred at 70 °C for 3–4 h. The mixture was then cooled to room temperature and poured in ice water. The precipitate formed was filtered, dried, and recrystallized from ethanol to give the corresponding 1*H*-1,2,4-triazole-3,5-diamine **2**.

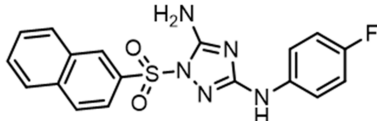
Synthesis of 1-Sulfonyl-3-amino-1*H*-1,2,4-triazoles **3 and **4**.** Substituted benzenesulfonyl chloride or naphthalene-sulfonyl chloride (1.0–1.2 equiv) was added to the suspension of the corresponding phenyl-1*H*-1,2,4-triazole-3,5-diamine **2** (1.0 equiv) in pyridine (5 mL), and the reaction mixture was stirred at room temperature overnight (12 h). The mixture was then diluted with water and stored in a refrigerator at 4 °C for 6–24 h. The resulting precipitate was filtered and purified as indicated below to give the corresponding final product.

1-((4-Fluorophenyl)sulfonyl)-*N*³-(naphthalen-1-yl)-1*H*-1,2,4-triazole-3,5-diamine **RCB14103**.



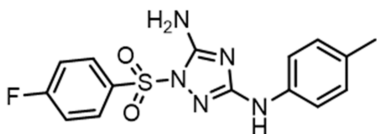
Yield 49%, mp 188–90 °C (EtOH). ¹H NMR (200 MHz; DMSO-*d*₆; δ , ppm; *J*, Hz): 7.44 (s, 2H, NH₂), 7.37–7.65 (m, 4H, HC(3'',4'',6'',7'')), 7.79 (d, 1H, HC(5''), *J* = 6.8), 7.87 (dd, 1H, HC(8''), *J* = 7.0, 1.8), 8.04 (dd, 2H, HC(2',6'), *J* = 8.9, 5.1), 8.15 (dd, 1H, HC(2''), *J* = 7.4, 1.8), 9.07 (s, 1H, NH). ¹³C NMR (50 MHz; DMSO-*d*₆; δ , ppm): 116.07 (C(2'')), 117.08 (d, C(3',5'), *J* = 22.2), 122.16 (C(8'')), 122.45 (C(4'')), 125.16 (C(8a'')), 125.79 (C(3'',6'',7'')), 127.96 (C(5'')), 130.70 (d, C(2',6'), *J* = 10.0), 132.28 (d, C(1'), *J* = 3.0), 133.71 (C(4a'')), 135.71 (C(1'')), 157.71 (C(5)), 161.16 (C(3)), 165.50 (d, C(4'), *J* = 253.0). MS (EI): *m/z* 383. Anal. Calcd for C₁₈H₁₄FN₃O₂S: C, 56.39; H, 3.68; N, 18.27. Found: C, 56.47; H, 3.74; N, 18.24.

*N*³-(4-Fluorophenyl)-1-(naphthalen-2-ylsulfonyl)-1*H*-1,2,4-triazole-3,5-diamine **RCB16008**.



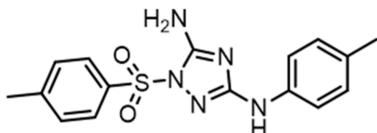
Yield 42%, mp 235–7 °C (EtOH/DMF). ¹H NMR (200 MHz; DMSO-*d*₆; δ, ppm; *J*, Hz): 7.08 (t, 2H, HC(3'',5''), *J* = 8.9), 7.45 (m, 4H, NH₂, HC(2'',6'')), 7.60–7.80 (m, 2H, HC(6',7')), 7.90 (dd, 1H, HC(8'), *J* = 8.7, 1.7), 8.05 (d, 1H, HC(3'), *J* = 7.2), 8.19 (d, 1H, HC(5'), *J* = 9.2), 8.24 (d, 1H, HC(4'), *J* = 7.1), 8.74 (s, 1H, HC(1')), 9.21 (s, 1H, NH). ¹³C NMR (50 MHz; DMSO-*d*₆; δ, ppm): 115.10 (d, *J* = 22.0), 117.93 (d, *J* = 7.5), 121.79, 127.95, 128.10, 129.47, 129.52, 129.77, 129.89, 131.37, 132.92, 134.99, 137.03 (d, *J* = 2.0), 156.31 (d, *J* = 235.0), 157.48, 159.75. MS (EI): *m/z* 383. Anal. Calcd for C₁₈H₁₄FN₅O₂S: C, 56.39; H, 3.68; N, 18.27. Found: C, 56.45; H, 3.73; N, 18.23.

1-((4-Fluorophenyl)sulfonyl)-*N*³-(*p*-tolyl)-1*H*-1,2,4-triazole-3,5-diamine **RCB16025**.



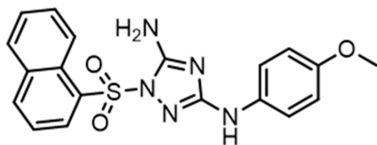
Yield 26%, mp 184–6 °C (column, hexane/ethyl acetate 1:1). ¹H NMR (200 MHz; DMSO-*d*₆; δ, ppm; *J*, Hz): 2.21 (s, 3H, CH₃), 7.04 (d, 2H, HC(3'',5''), *J* = 8.4), 7.34 (d, 2H, HC(2'',6''), *J* = 8.5), 7.38 (s, 2H, NH₂), 7.53 (t, 2H, HC(3',5'), *J* = 8.8), 7.90–8.12 (dd, 2H, HC(2',6'), *J* = 5.0, 8.9), 9.09 (s, 1H, NH). ¹³C NMR (50 MHz; DMSO-*d*₆; δ, ppm): 20.22, 116.67, 116.99 (d, *J* = 25.4), 128.86, 129.01, 130.62 (d, *J* = 10.5), 132.22 (d, *J* = 4.2), 138.07, 157.42, 160.00, 162.91, 165.44 (d, *J* = 252.0). MS (EI): *m/z* 347. Anal. Calcd for C₁₅H₁₄FN₅O₂S: C, 51.87; H, 4.06; N, 20.16. Found: C, 51.95; H, 4.11; N, 20.20.

*N*³-(*p*-Tolyl)-1-tosyl-1*H*-1,2,4-triazole-3,5-diamine **RCB16036**.



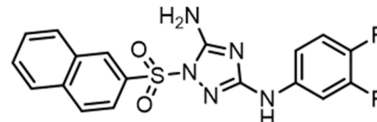
Yield 23%, mp 202–4 °C (*i*PrOH). ¹H NMR (200 MHz; DMSO-*d*₆; δ, ppm; *J*, Hz): 2.21 (s, 3H, H₃C(C4'')), 2.37 (s, 3H, H₃C(C4')), 7.03 (d, 2H, HC(3'',5''), *J* = 8.4), 7.32 (s, 2H, NH₂), 7.34 (d, 2H, HC(2'',6''), *J* = 8.2), 7.45 (d, 2H, HC(3',5'), *J* = 8.3), 7.83 (d, 2H, HC(2',6'), *J* = 8.3), 9.05 (s, 1H, NH). ¹³C NMR (50 MHz; DMSO-*d*₆; δ, ppm): 20.22, 21.07, 116.62, 127.34, 128.77, 128.98, 130.01, 133.07, 138.15, 145.63, 157.42, 159.82. MS (EI): *m/z* 343. Anal. Calcd for C₁₆H₁₇N₅O₂S: C, 55.96; H, 4.99; N, 20.39. Found: C, 56.02; H, 5.04; N, 20.34.

*N*³-(4-Methoxyphenyl)-1-(naphthalen-1-ylsulfonyl)-1*H*-1,2,4-triazole-3,5-diamine **RCB16086**.



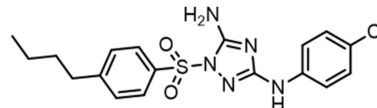
Yield 26%, mp 201–2 °C (hexane/ethyl acetate). ¹H NMR (200 MHz; DMSO-*d*₆; δ, ppm; *J*, Hz): 3.69 (s, 3H, CH₃), 6.80 (d, 2H, HC(3'',5''), *J* = 9.0), 7.29 (d, 2H, HC(2'',6''), *J* = 9.0), 7.40 (s, 2H, NH₂), 7.61–7.85 (m, 3H, HC(3',6',7')), 8.11 (d, 1H, HC(5'), *J* = 7.6), 8.38 (d, 1H, HC(4'), *J* = 8.2), 8.43 (d, 1H, HC(8'), *J* = 8.3), 8.88 (s, 1H, NH), 8.96 (d, 1H, HC(2'), *J* = 8.5). ¹³C NMR (50 MHz; DMSO-*d*₆; δ, ppm): 56.77, 113.80, 117.82, 121.75, 122.16, 124.61, 124.83, 127.77, 128.97, 129.29, 132.00, 133.68, 133.92, 136.23, 136.49, 156.33, 159.15. MS (EI): *m/z* 395. Anal. Calcd for C₁₉H₁₇N₅O₃S: C, 57.71; H, 4.33; N, 17.71. Found: C, 57.75; H, 4.26; N, 17.67.

*N*³-(3,4-Difluorophenyl)-1-(naphthalen-2-ylsulfonyl)-1*H*-1,2,4-triazole-3,5-diamine **RCB16178**.



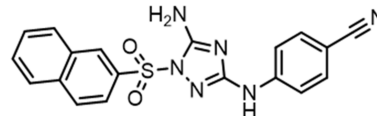
Yield 23%, mp 228–30 °C (column, hexane/ethyl acetate 6:4). ¹H NMR (200 MHz; DMSO-*d*₆; δ, ppm; *J*, Hz): 7.10–7.20 (m, 1H, HC(5'')), 7.29 (q, 1H, HC(2''), *J* = 9.3), 7.50 (s, 2H, NH₂), 7.56 (dd, *J* = 7.3, 2.5 Hz, 1H, HC(6'')), 7.65–7.82 (m, 2H, HC(6',7')), 7.89 (dd, 1H, HC(4'), *J* = 9.0, 1.7), 8.06 (d, 1H, HC(5'), *J* = 7.4), 8.19 (d, 1H, HC(3'), *J* = 8.7), 8.23 (d, 1H, HC(8'), *J* = 7.4), 8.74 (s, 1H, HC(1')), 9.44 (s, 1H, NH). ¹³C NMR (50 MHz; DMSO-*d*₆; δ, ppm): 105.17 (d, *J* = 22.1), 112.66 (dd, *J* = 2.6, 6.0), 117.31 (d, *J* = 18.0), 121.70, 127.97, 128.13, 129.52, 129.86, 129.94, 131.37, 132.92, 135.02, 137.77 (dd, *J* = 2.6, 9.1), 143.35 (dd, *J* = 13.0, 238.0), 148.88 (dd, *J* = 14.0, 252.0), 159.40. MS (EI): *m/z* 401. Anal. Calcd for C₁₈H₁₃F₂N₅O₂S: C, 53.86; H, 3.26; N, 17.45. Found: C, 53.91; H, 3.316; N, 17.39.

1-((4-Butylphenyl)sulfonyl)-*N*³-(4-chlorophenyl)-1*H*-1,2,4-triazole-3,5-diamine **RCB16185**.



Yield 25%, mp 156–8 °C (column hexane/ethyl acetate 6:4). ¹H NMR (200 MHz; DMSO-*d*₆; δ, ppm; *J*, Hz): 0.85 (t, 3H, CH₃, *J* = 7.2), 1.25 (h, 2H, H₂C(C3'')), 1.53 (p, 2H, H₂C(C2'')), *J* = 8.1, 7.4), 2.64 (t, 2H, H₂Car, *J* = 7.6), 7.28 (d, 2H, HC(2'',6''), *J* = 8.9), 7.37 (s, 2H, NH₂), 7.47 (d, 4H, HC(3',5',3'',5''), *J* = 9.2), 7.86 (d, 2H, HC(2', 6'), *J* = 8.3), 9.36 (brs, 1H, NH). ¹³C NMR (50 MHz; DMSO-*d*₆; δ, ppm): 13.58, 21.65, 32.34, 34.60, 118.06, 123.64, 127.42, 128.43, 129.42, 133.28, 139.59, 150.24, 157.31, 159.42. MS (EI): *m/z* 405. Anal. Calcd for C₁₈H₂₀ClN₅O₂S: C, 53.26; H, 4.97; N, 17.25. Found: C, 53.32; H, 5.03; N, 17.29.

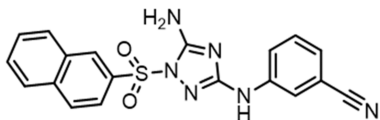
4-((5-Amino-1-(naphthalen-2-ylsulfonyl)-1*H*-1,2,4-triazol-3-yl)amino)benzonitrile **RCB17017**.



Yield 31%, mp 228–9 °C (CHCl₃). ¹H NMR (200 MHz; DMSO-*d*₆; δ, ppm; *J*, Hz): 7.55 (s, 2H, NH₂), 7.58 (d, 2H, HC(2'',6''), *J* = 8.8), 7.68 (d, 2H, HC(3'',5''), *J* = 8.8), 7.72–7.81 (m, 2H, HC(6',7')), 7.90 (dd, 1H, HC(8'), *J* = 8.7, 2.1), 8.05 (d, 1H, HC(3'), *J* = 7.3), 8.19 (d, 1H, HC(5'), *J* = 9.0), 8.24 (d, 1H, HC(4'), *J* = 7.9), 8.76 (s, 1H, HC(1')), 9.86 (s, 1H, NH). ¹³C NMR (50 MHz; DMSO-*d*₆; δ, ppm): 101.42,

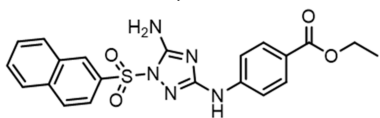
116.62, 119.55, 121.69, 127.97, 128.16, 129.55, 129.92, 130.00, 131.35, 132.82, 133.17, 135.04, 144.65, 157.35, 159.00. MS (EI): *m/z* 390. Anal. Calcd for C₁₉H₁₄N₆O₂S: C, 58.45; H, 3.61; N, 21.53. Found: C, 58.50; H, 3.67; N, 21.58.

3-((5-Amino-1-(naphthalen-2-ylsulfonyl)-1H-1,2,4-triazol-3-yl)amino)benzonitrile **RCB17019**.



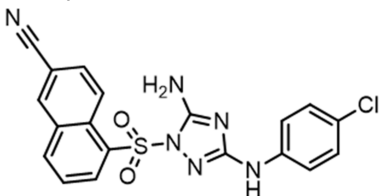
Yield 19%, mp 237–9 °C (EtOH). ¹H NMR (200 MHz; DMSO-*d*₆; δ, ppm; *J*, Hz): 7.27 (d, 1H, HC(6''), *J* = 7.6), 7.44 (t, 1H, HC(5''), *J* = 7.9), 7.54 (brs, 2H, NH₂), 7.64–7.81 (m, 3H, HC(6',7,4'')), 7.83 (s, 1H, HC(2'')), 7.90 (dd, 1H, HC(4'), *J* = 8.8, 1.8), 8.06 (d, 1H, HC(5'), *J* = 7.3), 8.19 (d, 1H, HC(3'), *J* = 8.3), 8.23 (d, 1H, HC(8'), *J* = 8.6), 8.74 (d, 1H, HC(1'), *J* = 1.7), 9.65 (brs, 1H, NH). ¹³C NMR (50 MHz; DMSO-*d*₆; δ, ppm): 111.40, 118.84, 119.03, 121.16, 121.72, 123.55, 127.98, 128.16, 129.52, 129.87, 129.98, 130.07, 131.37, 132.92, 135.04, 141.39, 157.41, 159.27. MS (EI): *m/z* 390. Anal. Calcd for C₁₉H₁₄N₆O₂S: C, 58.45; H, 3.61; N, 21.53. Found: C, 58.52; H, 3.64; N, 21.48.

4-((5-Amino-1-(naphthalen-2-ylsulfonyl)-1H-1,2,4-triazol-3-yl)amino)benzoic Acid Ethyl Ester **RCB17024**.



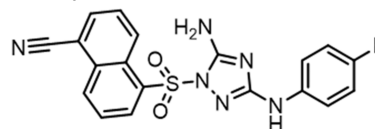
Yield 36%, mp 232–4 °C (CH₃CN). ¹H NMR (200 MHz; DMSO-*d*₆; δ, ppm; *J*, Hz): 1.29 (t, 3H, CH₃, *J* = 7.1), 4.25 (q, 2H, CH₂, *J* = 7.1), 7.53 (m, 4H, HC(3'',5''), NH₂), 7.65–7.74 (m, 2H, HC(6',7'')), 7.84 (d, 2H, HC(2'',6''), *J* = 8.8), 7.93 (dd, 1H, HC(8'), *J* = 8.7, 1.8), 8.05 (d, 1H, HC(3'), *J* = 7.2), 8.19 (d, 1H, HC(5'), *J* = 9.0), 8.25 (d, 1H, HC(4'), *J* = 7.4), 8.77 (s, 1H, HC(1')), 9.71 (s, 1H, NH). ¹³C NMR (50 MHz; DMSO-*d*₆; δ, ppm): 14.21, 60.09, 115.91, 121.10, 121.79, 127.95, 128.13, 129.56, 129.86, 129.98, 130.29, 131.38, 132.86, 135.04, 144.89, 157.36, 159.21, 165.46. MS (EI): *m/z* 437. Anal. Calcd for C₂₁H₁₉N₅O₄S: C, 57.66; H, 4.38; N, 16.01. Found: C, 57.71; H, 4.45; N, 16.05.

5-((5-Amino-3-(4-chlorophenyl)amino)-1H-1,2,4-triazol-1-yl)sulfonyl)-2-naphthonitrile **RCB17099**.



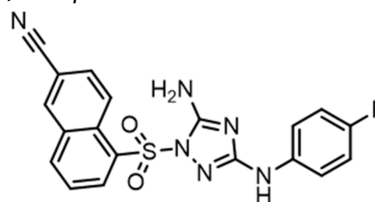
Yield 17%, mp 215–7 °C (column, CHCl₃/MeOH 9:1). ¹H NMR (200 MHz; DMSO-*d*₆; δ, ppm; *J*, Hz): 7.28 (d, 2H, HC(3'',5''), *J* = 9.1), 7.38 (d, 2H, HC(2'',6''), *J* = 9.1), 7.53 (s, 2H, NH₂), 7.93 (t, 1H, HC(7'), *J* = 7.9), 8.16 (d, 1H, HC(3'), *J* = 8.9), 8.49 (d, 1H, HC(8'), *J* = 8.0), 8.62 (d, 1H, HC(6'), *J* = 7.5), 8.78 (s, 1H, HC(1')), 9.13 (d, 1H, HC(4'), *J* = 9.1), 9.34 (s, 1H, NH). ¹³C NMR (50 MHz; DMSO-*d*₆; δ, ppm): 110.02, 117.95, 118.18, 123.76, 126.43, 126.61, 128.40, 128.54, 128.85, 132.18, 132.76, 133.46, 135.31, 136.88, 139.28, 156.44, 159.03. MS (EI): *m/z* 424. Anal. Calcd for C₂₁H₁₃ClN₅O₂S: C, 53.71; H, 3.08; N, 19.78. Found: C, 53.79; H, 3.13; N, 19.74.

5-((5-Amino-3-(4-fluorophenyl)amino)-1H-1,2,4-triazol-1-yl)sulfonyl)-1-naphthonitrile **RCB17150**.



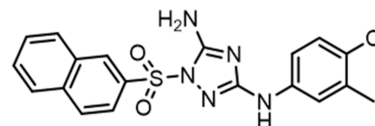
Yield 21%, mp 228–30 °C (EtOH). ¹H NMR (200 MHz; DMSO-*d*₆; δ, ppm; *J*, Hz): 7.08 (t, 2H, HC(3'', 5''), *J* = 8.9), 7.38 (dd, 2H, HC(2'',6''), *J* = 9.1, 4.8), 7.51 (s, 2H, NH₂), 7.91–8.10 (m, 2H, HC(3',7')), 8.35 (d, 1H, HC(2'), *J* = 7.2), 8.53 (d, 1H, HC(6'), *J* = 8.5), 8.62 (d, 1H, HC(8'), *J* = 7.5), 9.21 (s, 1H, NH), 9.38 (d, 1H, HC(4'), *J* = 8.8). ¹³C NMR (50 MHz; DMSO-*d*₆; δ, ppm): 116.02, 121.15, 122.69, 123.60, 123.75, 130.75, 132.48, 133.52, 133.73, 133.78, 136.45, 137.79, 138.06, 138.27, 138.88, 140.48, 142.60, 159.84, 162.32, 163.29, 165.11. MS (EI): *m/z* 408. Anal. Calcd for C₁₉H₁₃FN₆O₂S: C, 55.88; H, 3.21; N, 20.58. Found: C, 55.95; H, 3.26; N, 20.63.

5-((5-Amino-3-(4-fluorophenyl)amino)-1H-1,2,4-triazol-1-yl)sulfonyl)-2-naphthonitrile **RCB17153**.



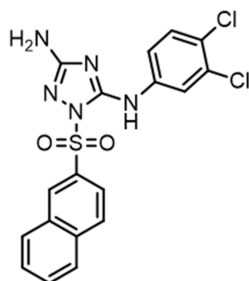
Yield 20%, mp 213–5 °C (column, CHCl₃/CH₃OH 9:1). ¹H NMR (200 MHz; DMSO-*d*₆; δ, ppm; *J*, Hz): 7.08 (t, 2H, HC(3'',5''), *J* = 8.9), 7.36 (dd, 2H, HC(2'',6''), *J* = 9.1, 4.7), 7.50 (brs, 2H, NH₂), 7.93 (t, 1H, HC(7'), *J* = 7.8), 8.14 (dd, 1H, HC(3'), *J* = 9.1, 1.9), 8.50 (d, 1H, HC(8'), *J* = 8.2), 8.61 (d, 1H, HC(6'), *J* = 7.4), 8.78 (d, 1H, HC(1'), *J* = 1.8), 9.14 (d, 1H, HC(4'), *J* = 9.0), 9.19 (s, 1H). ¹³C NMR (126 MHz; DMSO-*d*₆; δ, ppm): 110.55, 115.54 (d, *J* = 9.0), 118.40 (d, *J* = 2.5), 118.70, 121.15, 126.98, 127.12, 129.28, 129.86, 132.82, 133.29, 133.93, 135.80, 137.34, 156.86 (d, *J* = 224.0), 157.75, 159.80. MS (EI): *m/z* 408. Anal. Calcd for C₁₉H₁₃FN₆O₂S: C, 55.88; H, 3.21; N, 20.58. Found: C, 55.94; H, 3.24; N, 20.51.

*N*³-(4-Chloro-3-methylphenyl)-1-(naphthalen-2-ylsulfonyl)-1H-1,2,4-triazole-3,5-diamine **RCB17154**.



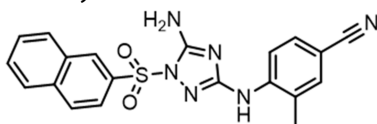
Yield 20%, mp 218–20 °C (*i*PrOH/DMF). ¹H NMR (200 MHz; DMSO-*d*₆; δ, ppm; *J*, Hz): 2.23 (s, 3H, CH₃), 7.24 (d, 1H, HC(5''), *J* = 8.7), 7.32 (s, 1H, HC(2'')), 7.34 (dd, 1H, HC(6''), *J* = 2.5, 8.7), 7.46 (brs, 2H, NH₂), 7.70–7.84 (m, 2H, HC(6',7')), 7.90 (dd, 1H, HC(4'), *J* = 8.7, 1.8), 8.05 (d, 1H, HC(5'), *J* = 7.2), 8.18 (d, 1H, HC(3'), *J* = 8.3), 8.23 (d, 1H, HC(8'), *J* = 8.6), 8.74 (d, 1H, HC(1'), *J* = 1.7), 9.26 (brs, 1H, NH). ¹³C NMR (50 MHz; DMSO-*d*₆; δ, ppm): 19.91, 115.79, 118.94, 121.81, 124.04, 127.95, 128.10, 128.84, 129.52, 129.77, 129.90, 131.36, 132.93, 135.01, 135.16, 139.50, 157.39, 159.54. MS (EI): *m/z* 413. Anal. Calcd for C₁₉H₁₆ClN₅O₂S: C, 55.14; H, 3.90; N, 16.92. Found: C, 55.21; H, 3.98; N, 16.87.

*N*⁵-(3,4-Dichlorophenyl)-1-(naphthalen-2-ylsulfonyl)-1*H*-1,2,4-triazole-3,5-diamine **RCB17160**.



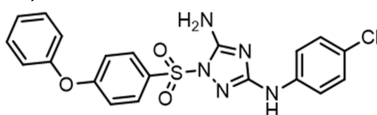
Yield 13%, mp 223–5 °C (column, CHCl₃/CH₃OH 9:1). ¹H NMR (200 MHz; DMSO-*d*₆; δ, ppm; *J*, Hz): 6.11 (brs, 2H, NH₂), 7.60 (d, 1H, HC(5''), *J* = 8.8), 7.66 (dd, 1H, HC(6''), *J* = 2.0, 8.8), 7.73–7.85 (m, 2H, HC(6',7')), 8.05 (d, 1H, HC(2''), *J* = 2.0), 8.07 (d, 1H, HC(5'), *J* = 7.5), 8.16 (d, 1H, HC(3'), *J* = 8.3), 8.20 (d, 1H, HC(8'), *J* = 8.6), 8.64 (s, 1H, HC(1')), 9.51 (s, 1H, NH). ¹³C NMR (50 MHz; DMSO-*d*₆; δ, ppm): 119.61, 120.52, 121.78, 124.52, 127.95, 128.10, 129.55, 129.82, 129.99, 130.50, 130.98, 131.35, 132.59, 135.03, 138.67, 154.39, 163.40. MS (EI): *m/z* 434. Anal. Calcd for C₁₈H₁₃Cl₂N₅O₂S: C, 49.78; H, 3.02; N, 16.13. Found: C, 49.85; H, 3.08; N, 16.07.

4-((5-Amino-1-(naphthalen-2-ylsulfonyl)-1*H*-1,2,4-triazol-3-yl)amino)-3-methylbenzonitrile **RCB17162**.



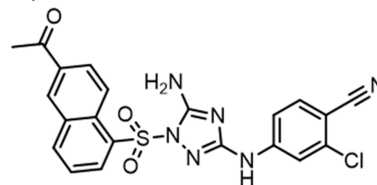
Yield 34%, mp 125–7 °C (EtOH). ¹H NMR (200 MHz; DMSO-*d*₆; δ, ppm; *J*, Hz): 2.18 (s, 3H, CH₃), 7.46–7.62 (m, 4H, NH₂, HC(2'',6'')), 7.66–7.84 (m, 2H, HC(6',7')), 7.90 (dd, 1H, HC(4'), *J* = 8.7, 1.8), 7.94 (d, 1H, HC(5''), *J* = 8.3), 8.07 (d, 1H, HC(5'), *J* = 7.2), 8.21 (d, 1H, HC(3'), *J* = 8.3), 8.25 (d, 1H, HC(8'), *J* = 8.2), 8.53 (s, 1H, NH), 8.75 (d, 1H, HC(1'), *J* = 1.7). ¹³C NMR (50 MHz; DMSO-*d*₆; δ, ppm): 17.48, 102.45, 118.09, 119.42, 121.70, 127.19, 127.98, 128.16, 129.58, 129.96 (2C), 130.67, 131.40, 132.94, 133.56, 135.07, 143.02, 157.42, 159.48. MS (EI): *m/z* 404. Anal. Calcd for C₂₀H₁₆N₆O₂S: C, 59.39; H, 3.99; N, 20.78. Found: C, 59.45; H, 4.04; N, 20.71.

*N*³-(4-Chlorophenyl)-1-((4-phenoxyphenyl)sulfonyl)-1*H*-1,2,4-triazole-3,5-diamine **RCB17166**.



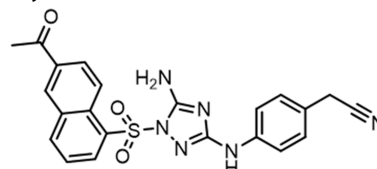
Yield 21%, mp 210–2 °C (CHCl₃, then CH₃CN). ¹H NMR (200 MHz; DMSO-*d*₆; δ, ppm; *J*, Hz): 7.10–7.21 (m, 4H, HC(3',5',2'',6'')), 7.23–7.29 (m, 3H, HC(3'',4'',5'')), 7.30 (s, 2H, NH₂), 7.40 (d, 2H, HC(3'',5''), *J* = 9.0), 7.44–7.51 (m, 4H, HC(2'',6'')), 7.95 (d, 2H, HC(2',6'), *J* = 8.8), 9.39 (s, 1H, NH). ¹³C NMR (50 MHz; DMSO-*d*₆; δ, ppm): 117.38, 118.08, 120.54, 123.64, 125.42, 128.45, 129.35, 130.19, 130.44, 139.59, 154.02, 157.22, 159.42, 162.51. MS (EI): *m/z* 441. Anal. Calcd for C₂₀H₁₆ClN₅O₃S: C, 54.36; H, 3.65; N, 15.85. Found: C, 54.41; H, 3.70; N, 15.88.

4-((1-((6-Acetylnaphthalen-1-yl)sulfonyl)-5-amino-1*H*-1,2,4-triazol-3-yl)amino)-2-chlorobenzonitrile **RCB22055**.



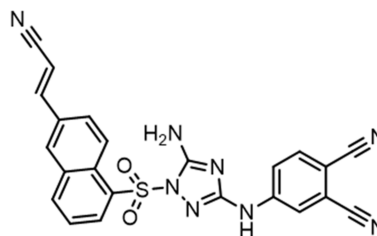
Yield 36%, mp 270–3 °C (column, CHCl₃/CH₃OH 9:1). ¹H NMR (200 MHz; DMSO-*d*₆; δ, ppm; *J*, Hz): 2.70 (s, 3H, CH₃), 7.36 (dd, 1H, HC(6''), *J* = 8.7, 2.2), 7.67 (s, 2H, NH₂), 7.73 (d, 1H, HC(2''), *J* = 2.2), 7.75 (d, 1H, HC(5''), *J* = 8.7), 7.88 (t, 1H, HC(3'), *J* = 7.9), 8.22 (dd, 1H, HC(7'), *J* = 9.1, 1.8), 8.60 (d, 2H, HC(2',4'), *J* = 7.7), 8.83 (d, 1H, HC(5'), *J* = 1.7), 8.99 (d, 1H, HC(8'), *J* = 9.0), 10.07 (s, 1H, NH). ¹³C NMR (50 MHz; DMSO-*d*₆; δ, ppm): 26.79, 101.84, 115.44, 116.22, 116.73, 124.80, 125.82, 126.31, 129.78, 131.14, 131.80, 133.14, 133.40, 134.92 (2C), 136.08, 138.25, 145.69, 156.45, 158.06, 197.45. MS (EI): *m/z* 466. Anal. Calcd for C₂₁H₁₅ClN₆O₃S: C, 54.02; H, 3.24; N, 18.00. Found: C, 54.11; H, 3.31; N, 18.06.

4-((1-((6-Acetylnaphthalen-1-yl)sulfonyl)-5-amino-1*H*-1,2,4-triazol-3-yl)amino)benzonitrile **RCB22056**.

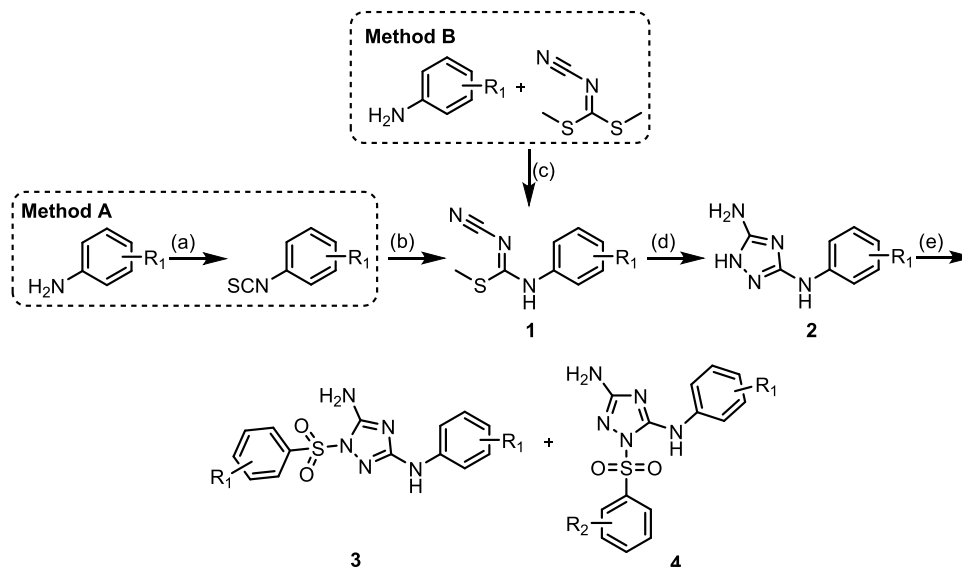


Yield 24%, mp 210–5 °C (column, CHCl₃/CH₃OH 9:1). ¹H NMR (200 MHz; DMSO-*d*₆; δ, ppm; *J*, Hz): 2.70 (s, 3H, CH₃), 3.89 (s, 2H, CH₂), 7.16 (d, 2H, HC(2'',6''), *J* = 8.4), 7.36 (d, 2H, HC(3'',5''), *J* = 8.4), 7.52 (brs, 2H, NH₂), 7.87 (t, 1H, HC(3'), *J* = 7.9), 8.19 (dd, 1H, HC(7'), *J* = 9.1, 1.8), 8.57 (d, 2H, HC(2',4'), *J* = 7.8), 8.82 (d, 1H, HC(5'), *J* = 1.8), 9.03 (d, 1H, HC(8'), *J* = 9.1), 9.23 (s, 1H, NH). ¹³C NMR (50 MHz; DMSO-*d*₆; δ, ppm): 21.68, 26.80, 116.88, 119.52, 122.52, 125.26, 125.77, 126.03, 128.37, 129.89, 130.99, 132.08, 132.95, 133.35, 134.83, 137.93, 139.93, 156.51, 159.09, 197.51. MS (EI): *m/z* 446. Anal. Calcd for C₂₂H₁₈N₆O₃S: C, 59.18; H, 4.06; N, 18.82. Found: C, 59.25; H, 4.13; N, 18.89.

4-((5-Amino-1-((6-(2-cyanovinyl)naphthalen-1-yl)sulfonyl)-1*H*-1,2,4-triazol-3-yl)amino)-2-ethynylbenzonitrile **RCB22057**.



Yield 19%, mp 298–300 °C (column, CHCl₃/CH₃OH 9:1). ¹H NMR (200 MHz; DMSO-*d*₆; δ, ppm; *J*, Hz): 6.67 (d, 1H, HC(2''), *J* = 16.7), 7.66–7.89 (m, 5H, HC(1'',3'',6'', NH₂)), 7.96 (d, 1H, HC(5''), *J* = 8.8), 8.10 (dd, 1H, HC(7'), *J* = 9.1, 1.8), 8.33 (d, 1H, HC(5'), *J* = 1.8), 8.41 (d, 1H, HC(2'), *J* = 8.2), 8.53 (d, 1H, HC(4'), *J* = 7.4), 8.87 (d, 1H, HC(8'), *J* = 9.1), 10.30 (s, 1H, NH). ¹³C NMR (50 MHz; DMSO-*d*₆; δ, ppm): 99.08, 103.94, 115.28, 116.16, 116.57, 118.46, 120.15 (2C), 124.83, 125.91, 125.97, 128.52, 130.22,

Scheme 1. Synthesis of 1-Sulfonyl-3-amino-1*H*-1,2,4-triazoles **3** and **4**^a

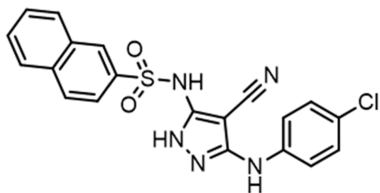
^a(a) Dimethylthiocarbonyl chloride, toluene, or benzene, reflux; (b) NaOEt, NH₂CN, MeI, EtOH, reflux; (c) EtOH, reflux; (d) hydrazine hydrate, EtOH, reflux; (e) PhSO₂Cl or NapSO₂Cl, pyridine, rt.

131.80, 132.28, 132.65, 133.65, 134.90, 137.32, 144.87, 149.24, 156.42, 157.88. MS (EI): *m/z* 466. Anal. Calcd for C₂₃H₁₃N₈O₂S: C, 59.22; H, 3.03; N, 24.02. Found: C, 59.31; H, 3.09; N, 24.05.

Synthesis of 5-Amino-3-(disubstituted phenylamino)-1*H*-pyrazole-4-carbonitriles **5.** A mixture of the corresponding aniline (1.0–1.2 equiv) and 2-(bis(methylthio)methylene)malononitrile (1.0 equiv) in EtOH (20 mL) was stirred at reflux for 3 h. After completion of the reaction (monitored by thin-layer chromatography (TLC) hexane/acetone 2:1), the mixture was cooled to room temperature. When a precipitate appeared, hydrazine hydrate (2.0–2.5 equiv) was added, and the reaction mixture was stirred at reflux for an additional 2 h. After the completion of the reaction, the mixture was cooled to room temperature and poured into cold water. The precipitate of the corresponding product was filtered, dried, and used without further purification.

Synthesis of *N*-(4-Cyano-3-(disubstituted phenylamino)-1*H*-pyrazol-5-yl)naphthalene-2-sulfonamides **6.** A mixture of naphthalenesulfonyl chloride (1.0–1.3 equiv) and the corresponding aminopyrazole (1.0 equiv) in pyridine (5 mL) was stirred at room temperature for 2–3 days. After completion of the reaction (monitored by TLC hexane/acetone 2:1), the mixture was poured into ice water, and the precipitate was filtered, dried, and recrystallized from ethanol to give the corresponding final product.

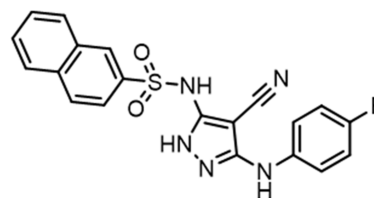
***N*-(3-((4-Chlorophenyl)amino)-4-cyano-1*H*-pyrazol-5-yl)naphthalene-2-sulfonamide **RCB16002**.**



Yield 18%, mp 226–9 °C. ¹H NMR (200 MHz; DMSO-*d*₆; δ, ppm; *J*, Hz): 7.27 (d, 2H, HC(3'',5''), *J* = 8.9), 7.50 (d, 2H, HC(2'',6''), *J* = 8.9), 7.63 (brs, 2H, 2NH), 7.67–7.83 (m, 2H, HC(6',7')), 7.89 (dd, 1H, HC(4'), *J* = 8.7, 1.9), 8.06 (d, 1H,

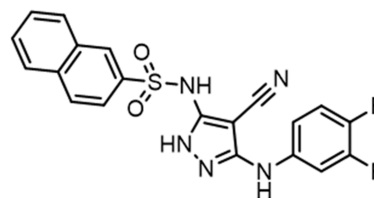
HC(5'), *J* = 7.2), 8.20 (d, 1H, HC(3'), *J* = 8.9), 8.25 (d, 1H, HC(8'), *J* = 7.6), 8.74 (d, 1H, HC(1'), *J* = 1.6), 8.89 (brs, 1H, NH). ¹³C NMR (50 MHz; DMSO-*d*₆; δ, ppm): 112.48, 119.04, 121.70, 124.40, 128.00, 128.19, 128.37, 129.61, 129.93, 130.08, 131.37, 132.40, 135.11, 139.50, 152.78, 156.02. MS (EI): *m/z* 423. Anal. Calcd for C₂₀H₁₄ClN₅O₂S: C, 56.67; H, 3.33; N, 16.52. Found: C, 56.73; H, 3.39; N, 16.48.

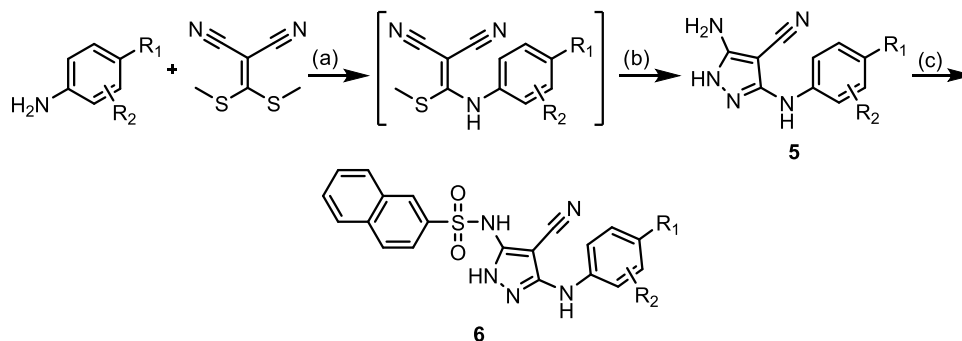
***N*-(4-Cyano-3-((4-fluorophenyl)amino)-1*H*-pyrazol-5-yl)naphthalene-2-sulfonamide **RCB16003**.**



Yield 59%, mp 175–7 °C. ¹H NMR (200 MHz; DMSO-*d*₆; δ, ppm; *J*, Hz): 7.09 (t, 2H, HC(3'',5''), *J* = 8.9), 7.52 (dd, 2H, HC(2'',6''), *J* = 9.0, 4.8), 7.66–7.83 (m, 4H, 2NH, HC(6',7')), 7.88 (dd, 1H, HC(8'), *J* = 8.7, 1.8), 8.07 (d, 1H, HC(3'), *J* = 7.2), 8.21 (d, 1H, HC(5'), *J* = 9.2), 8.26 (d, 1H, HC(4'), *J* = 7.2), 8.76 (s, 1H, HC(1')), 8.88 (s, 1H, NH). ¹³C NMR (50 MHz; DMSO-*d*₆; δ, ppm): 65.18, 112.57, 115.04 (d, *J* = 22.0), 119.11 (d, *J* = 7.5), 121.70, 128.00, 128.19, 129.59, 129.83, 129.91, 130.06, 131.37, 132.43, 135.10, 136.96, 153.08, 156.09, 156.70 (d, *J* = 237.0). MS (EI): *m/z* 407. Anal. Calcd for C₂₀H₁₄FN₅O₂S: C, 58.96; H, 3.46; N, 17.19. Found: C, 59.02; H, 3.52; N, 17.17.

***N*-(4-Cyano-3-((3,4-difluorophenyl)amino)-1*H*-pyrazol-5-yl)naphthalene-2-sulfonamide **RCB16004**.**



Scheme 2. Synthesis of 2-Sulfonyl-4-cyano-1H-pyrazoles 6^a

^a(a) EtOH, reflux; (b) hydrazine hydrate, EtOH, reflux; (c) NapSO₂Cl, pyridine, rt.

Table 1. *In Vitro* Effects of Phenylsulfonyl Aminotriazoles on YFV 17D Infection of Huh7 Cells

Compound	R ₁	R ₂	EC ₅₀ (YFV 17D, μM)	CC ₅₀ (Huh7, μM)	SI ₅₀
RCB14103	4-F		23.0	94.0	4.1
RCB16025	4-F	4-Me	> 32.0	32.0	< 1.0
RCB16036	4-Me	4-Me	> 100.0	> 100.0	< 1.0
RCB16185	4- ⁿ Bu	4-Cl	> 13.0	13.0	< 1.0
RCB17166	4-OPh	4-Cl	> 31.0	31.0	< 1.0
RCB20116 ^a		2-Cl, 4-CN	24.0	48.0	2.0

^aPreviously described.³⁵

Yield 21%, mp 239–42 °C. ¹H NMR (200 MHz; DMSO-*d*₆; δ, ppm; *J*, Hz): 7.20–7.40 (m, 2H, HC(2'',S'')), 7.50–7.65 (m, 1H, HC(6'')), 7.76 (s, 2H, 2NH), 7.67–7.82 (m, 1H, HC(S',6')), 7.87 (dd, 1H, HC(7'), *J* = 9.0, 1.9), 8.07 (d, 1H, HC(4'), *J* = 7.4), 8.20 (d, 1H, HC(3'), *J* = 8.1), 8.24 (d, 1H, HC(8'), *J* = 9.0), 8.76 (d, 1H, HC(1'), *J* = 1.5), 9.12 (s, 1H, NH). ¹³C NMR (50 MHz; DMSO-*d*₆; δ, ppm): 106.27 (d, *J* = 22.1), 112.42, 113.66 (dd, *J* = 2.7, 6.0), 117.23 (d, *J* = 17.5), 121.61, 128.01, 128.22, 129.58, 129.79, 130.01, 130.12, 131.34, 132.42, 135.13, 137.65 (dd, *J* = 2.6, 9.1), 143.88 (dd, *J* = 14.0, 254.0), 148.70 (dd, *J* = 14.0, 255.0), 152.69, 155.90. MS (EI): *m/z* 425. Anal. Calcd for C₂₀H₁₃F₂N₅O₂S: C, 56.47; H, 3.08; N, 16.46. Found: C, 56.53; H, 3.12; N, 16.48.

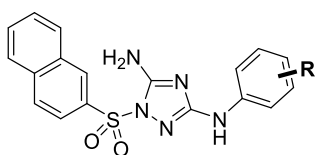
Yellow Fever Virus Inhibition Assay in Huh7 Cells. YFV inhibition assays were performed through the NIAID *In Vitro* Assessment for Antimicrobial Activity program and are detailed in the [Supporting Information](#). Briefly, compounds were tested for a cytopathic effect against YFV 19D-infected Huh7 cells. Four concentration assays were performed using Infergen as a positive control and visualized using a neutral red dye. EC₅₀ and CC₅₀ values were obtained by linear regression analysis and the selectivity index (SI) was calculated by dividing the EC₅₀ by the CC₅₀.

***In Vitro* ADME/Tox Assays.** *In vitro* ADME studies were performed by BioDuro (San Diego, CA) and fully described in the [Supporting Information](#). Kinetic solubility was calculated from the concentration of each compound in a Universal Aqueous buffer with reference to a standard curve. Caco-2

permeability was calculated by treating preincubated Caco-2 cells with each compound and measuring the change in concentration between the apical and basolateral sides of the cells. Human CYP inhibition was measured by liquid chromatography–mass spectrometry (LCMS) after treating each of the compounds with a human liver microsome solution. Mouse/human liver microsome stability and clearance were determined by LCMS analysis of each compound after treatment with a liver microsome solution. Plasma protein binding was determined by equilibrium dialysis using LCMS to measure the concentration. Cytotoxicity was determined by treating Huh-7D12 and THP-1 cells with each compound, and cell viability after 72 h was assessed by resazurin fluorescence. Mutagenicity was evaluated by *Escherichia coli* PQ37³⁶ using 4-nitroquinoline *N*-oxide as a positive control. Pharmacokinetic studies were performed using male Balb/C mice blood, brain, and liver samples collected up to 24 h after intragastric dosing of each compound.

RESULTS

Synthesis of Target Compounds. The target compounds were synthesized according to [Schemes 1 and 2](#). The key intermediate *N*'-cyano-*N*-substituted phenylcarbamidithioic acid methyl esters **1** can be synthesized by two different methods ([Scheme 1](#)). Method A is a two-step process involving the preparation of aryl thiocyanates, followed by treatment with sodium ethoxide and cyanamide. Method B

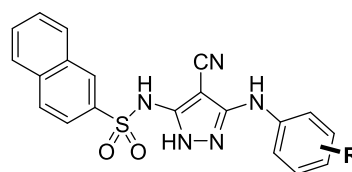
Table 2. *In Vitro* Effects of 2-Naphthalenesulfonyl Aminotriazoles on the YFV 17D Infection of Huh7 Cells

compound	R	EC ₅₀ (YFV 17D, μM)	CC ₅₀ (Huh7, μM)	SI ₅₀
RCB16007	4-Cl	3.3	32	9.7
RCB16008	4-F	>32.0	32.0	<1.0
RCB16178	3,4-F	>31.0	31.0	<1.0
RCB17017	4-CN	>32.0	32.0	<1.0
RCB17019	3-CN	19.0	>100.0	>5.3
RCB17024	4-CO ₂ Me	2.6	22.0	8.5
RCB17154	3-Me, 4-Cl	4.1	28.0	6.8
RCB17158 ^a	3-Cl, 4-CN	4.0	31.0	7.8
RCB17160 ^b	3,4-Cl	>100.0	>100.0	1.0
RCB17162	2-Me, 4-CN	8.1	70.0	8.6
RCB18320 ^{a,c}	4-Cl	7.7	31.0	4.0

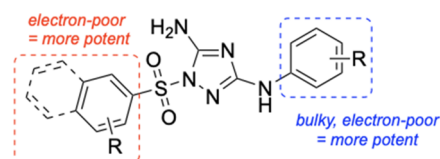
^aPreviously described.³⁵ ^bAryl ring on other NH₂. ^c6-Cl naphthyl group.

consists of a direct reaction of the corresponding aniline with dimethyl cyanocarbonimidodithioate. The *N'*-cyano-*N*-substituted phenylcarbamimidodithioic acid methyl esters **1** were then allowed to react with hydrazine hydrate to cyclize into a 1,2,4-triazole ring. Treatment of the corresponding substituted phenyl-1*H*-1,2,4-triazole-3,5-diamines **2** with various arylsulfonyl chlorides afforded the final triazoles **3**. In some cases, we were also able to isolate another isomer by column chromatography (compound **RCB17160**). According to [Scheme 2](#), the intermediate 4-cyano-5-amino-3-(phenylamino)-1*H*-pyrazoles **5** were prepared *in situ* after treatment of the aniline and malononitrile reaction mixture with hydrazine hydrate. Subsequent treatment of **5** with naphthalenesulfonyl chloride resulted in the target pyrazoles **6**.

Antiviral Activity. The synthesized triazoles and pyrazoles were then tested for their activity against YFV-infected Huh7 cells. The *in vitro* antiviral activity was assayed by neutral red

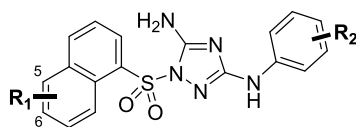
Table 4. *In Vitro* Effects of Aminopyrazoles on YFV 17D Infection of Huh7 Cells

compound	R	EC ₅₀ (YFV 17D, μM)	CC ₅₀ (Huh7, μM)	SI ₅₀
RCB16002	4-Cl	7.1	32.0	4.5
RCB16004	3,4-F	>36.0	36.0	<1.0

**Figure 1. SAR Summary of functional group effects on the compound potency.**

dye uptake, using Inergen as the positive control (EC₅₀ < 0.01 ng/mL, CC₅₀ > 10 ng/mL). The activities of the compounds against YFV are shown in [Tables 1–4](#), separated based on structural modifications.

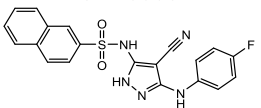
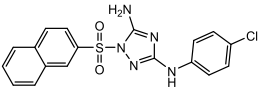
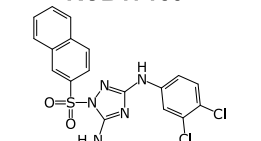
Structure–Activity Relationship (SAR). After identification of the initial hit compound **RCB16007**, we explored the SAR of this structure by testing a panel of compounds, which we had previously synthesized as part of our ongoing HIV program.³⁵ These compounds are composed of either a 1,2,4-triazole ring or a pyrazole ring between a functionalized aniline moiety and an arylsulfonyl moiety. A summary of the SAR is shown in [Figure 1](#). Of the tested compounds, those bearing more electron-withdrawing groups on the aniline ring exhibited greater potency, with the exception of the difluoro-containing compound **RCB16178**. Aniline fragments bearing two cyano substituents, such as **RCB22057**, were also more active, supporting the idea that electron-deficient yet sterically bulky aniline rings are important for potency. For example, compound **RCB22055**, which bears electron-withdrawing

Table 3. *In Vitro* Effects of 1-Naphthalenesulfonyl Aminotriazoles on YFV 17D Infection of Huh7 Cells

compound	R ₁	R ₂	EC ₅₀ (YFV 17D, μM)	CC ₅₀ (Huh7, μM)	SI ₅₀
RCB16086		4-OMe	32.0	>100.0	>3.1
RCB17099	6-CN	4-Cl	3.6	29.0	8.1
RCB17150	5-CN	4-F	2.9	26.0	9.0
RCB17152 ^a	6-CN	4-CN	>100.0	>100.0	1.0
RCB17153	6-CN	4-F	14.0	27.0	1.9
RCB20108 ^a	6-CN	2,4,6-Cl	>100.0	>100.0	1.0
RCB21055 ^a	6-CN	3,4-CN	5.2	11.0	2.1
RCB21065 ^a	6-CH=CHCN	3-Cl, 4-CN	>17.0	17.0	<1.0
RCB21066 ^a	6-CH=CHCN	4-CH ₂ CN	>29.0	29.0	<1.0
RCB22055	6-Ac	3-Cl, 4-CN	1.3	9.9	7.6
RCB22056	6-Ac	4-CH ₂ CN	>17.0	17.0	<1.0
RCB22057	6-CH=CHCN	3,4-CN	2.8	37.0	13.0

^aPreviously described.³⁵

Table 5. Secondary *In Vitro* Antiviral Screening Results against YFV (17D) for Compounds RCB16003, RCB16007, and RCB17159 in Huh7 Cells

Compound	EC ₅₀ , μM	EC ₉₀ (VYR), μM	CC ₅₀ , μM	SI ₅₀	SI ₉₀
RCB16003^a 	6.1	8.5	24.0	3.9	2.8
RCB16007^a 	6.1	11.0	28.0	4.6	2.5
RCB17159^a 	5.6	3.5	16.0	2.9	4.6

^aPrimary inhibition data for this compound published previously.³¹ VYR = virus yield reduction. Infergen was used as a positive control with EC₅₀ 50 > 10 ng/mL. ^bPreviously described.³⁵

Table 6. Summary of ADME Data for Compound RCB16007

ADME property	value
solubility	<0.2 μM
CYP inhibition IC ₅₀	1A2 (11.1 μM), 2C9 (26.5 μM), 2C19 (8.78 μM), 3A4 and 2D6 (>50 μM)
mouse liver microsomes	<i>t</i> _{1/2} 66.6 min, CL _{int} 10.4 μL/min/mg protein, stable
human liver microsomes	<i>t</i> _{1/2} 347 min, CL _{int} 2.0 μL/min/mg protein, stable
mouse plasma protein binding	>99.9%
human plasma protein binding	>99.9%
Caco-2	<i>P</i> _{app} A–B = 0.138; B–A = 0.122 (×10 ^{−6} cm/s), efflux ratio = 0.883
HERG	>10 μM

chloro and cyano groups, displays low micromolar activity, while RCB22056, which bears an acetonitrile group on the aniline, is inactive. Similarly, electron-withdrawing groups on the sulfonyl arene moiety exhibit more potency with electron-rich arenes, such as those present in RCB16086, resulting in a complete loss of potency. The presence of a naphthalene ring in the sulfonyl moieties was generally more active than those containing a single aromatic ring, and more so with more strongly electron-withdrawing substituents such as cyano and acrylonitrile groups. Compound RCB17160, in which the aniline and sulfonyl moieties are on adjacent atoms in the triazole and pyrazole rings, did not display any activity. While this supports the requirement for 1,3-substituted triazoles, more analogues are needed to gauge the role of the 1,3-pyrazole core. Lastly, we did not see a significant difference in the role of the pyrazole versus the triazole scaffold. Pyrazoles RCB16002 and RCB16004 showed similar activity to the analogous triazoles RCB16178 and RCB18320, supporting that both heterocyclic cores are potential anti-YFV scaffolds.

Overall, these analogues suggest that both the aniline and arylsulfonyl moieties are quite sensitive to substitutions. However, we have been able to improve compounds from our initial screen with compound RCB17159 displaying a 3-fold increase in activity and a similar 3-fold improvement in SI relative to that of RCB16007 in a primary screen. Compound RCB22055 displays similar antiviral activity with a slightly lower SI.

Secondary *In Vitro* Testing. We previously identified RCB16003 after prioritizing compounds in our library using a machine learning model for YFV (Tables 1–4). Based on our initial hit, we undertook secondary testing on RCB16003, RCB16007 (initial lead compound against HIV), and RCB17159, as they had the best SI in the primary screen. These results suggested that these compounds all had similar *in vitro* performance against YFV (Table 5).

***In vitro* ADME/Tox for RCB16007.** We were keen to understand the *in vitro* ADME/Tox properties of this class of compounds and selected compound RCB16007 as a promising representative, as shown in Table 6. While we observed poor solubility and slight CYP2C19 inhibition, RCB16007 displayed good human and mouse liver microsomal stability, and no signs of efflux in Caco-2 cells (Table 3). Also, this compound at 10 mg/mL did not appear to be mutagenic in *E. coli* PQ37 in the SOS-chromotest assay, compared with the control 4NQO. The TD₉₉ in THP-1 and Huh-7D12 was >11 μg/mL. We have previously determined that this molecule additionally had no inhibition of hERG (>10 μM).³⁵

Preliminary *In Vivo* Toxicity and Pharmacokinetic Studies for RCB16007. Toxicity studies on mice revealed that the LD₅₀ value for RCB16007 was 3930 mg/kg, allowing it to be classified as “nontoxic”. A single-dose PK study in mice with intragastrically administered RCB16007 at a dose of 250 mg/kg showed a *T*_{1/2} value of 3.4 h and a *C*_{max} value of 1190 ng/mL, suggesting it has good bioavailability (Figure 2).

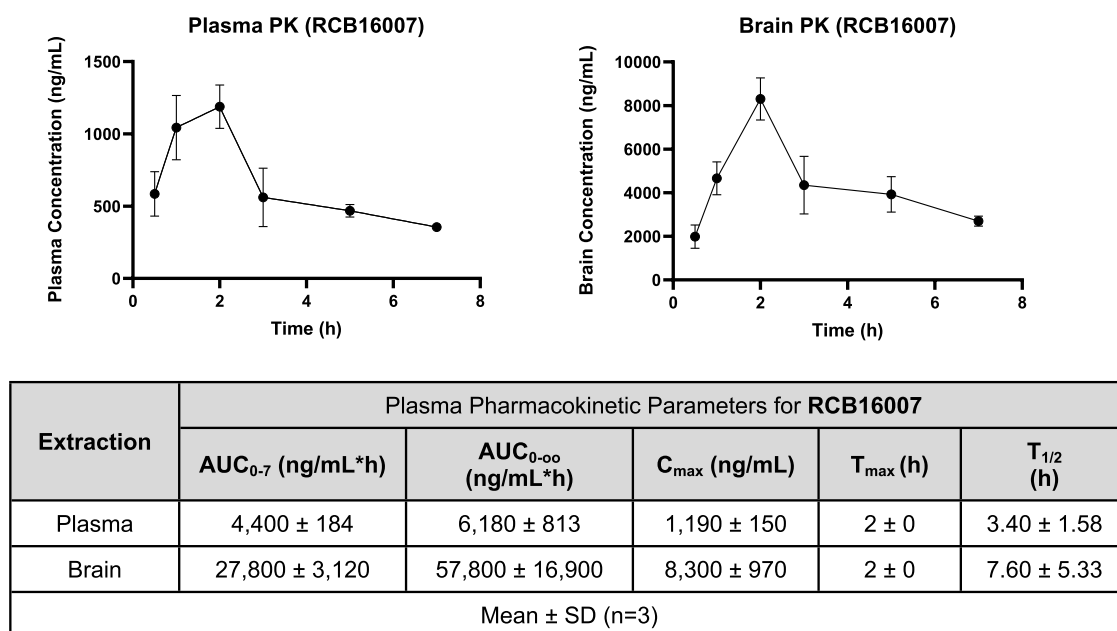


Figure 2. Pharmacokinetic data for mice dosed with 250 mg/kg of RCB16007 via intragastric intubation administration in either plasma (left) or brain (right). Pharmacokinetic parameters were calculated with a Noncompartmental Pharmacokinetics Analysis method. Error bars represent standard deviation (SD).

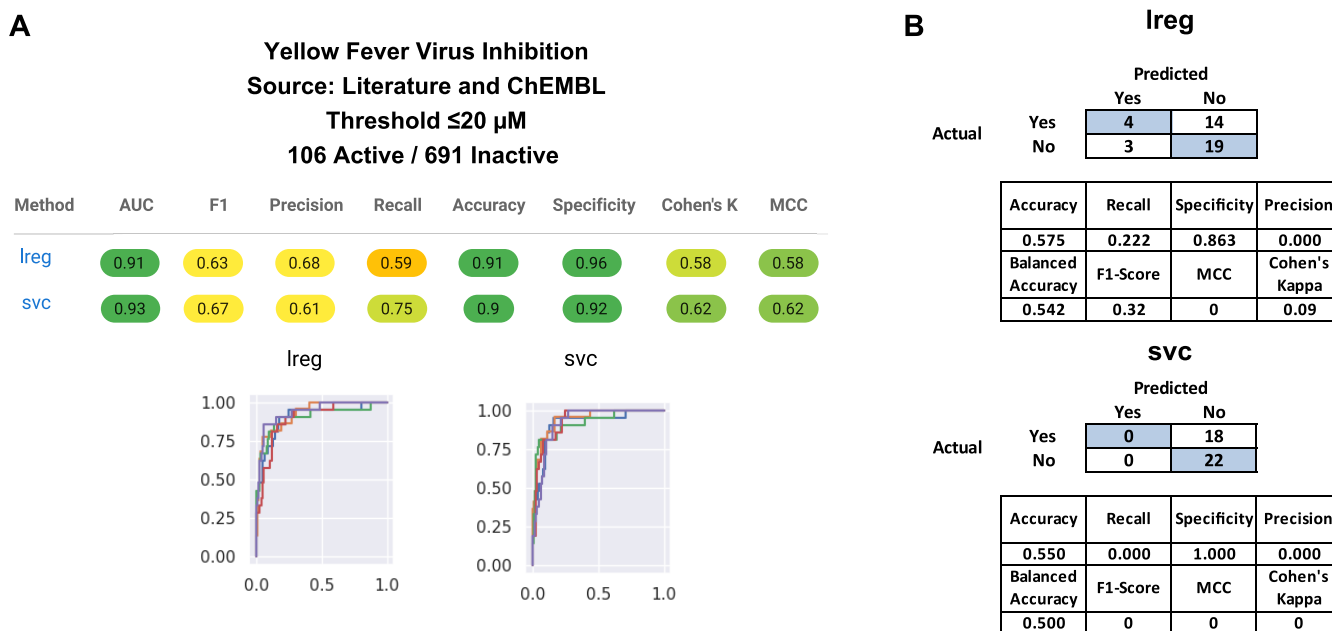


Figure 3. Representative CV (A) and external test set (B) statistics for models built using lreg and svc (20 μM threshold).

Machine Learning and Predictions. We have rebuilt our YFV machine learning models using the most recent version of our proprietary Assay Central software from the data set and thresholds from our previously published paper.²⁹ The new models overall showed good cross-validation statistics using these additional algorithms (Figure S1) and performed similarly to the original models. This data set was expanded to include more recent publicly available data from ChEMBL with classification models built using the activity thresholds of 10 and 20 μM . While the training data sets were quite unbalanced (60/701 or 106/691 active/inactives), several algorithms had reasonable CV scores, with knn, lreg, and svc performing well at both thresholds (Figure S2). To addition-

ally attempt to validate these models, we used our novel class of compounds as an external validation set. Cross-validation and external test stats for models built using two of the best performing algorithms, lreg and svc, are shown in Figure 3. While CV statistics suggested that these were predictive models, the external test set validation scores strongly suggest that these models are not able to predict our new class of yellow fever virus inhibitors. Based on this poor performance, models were also built with the currently generated data only. While the training data are small (40 compounds), some of these models showed surprisingly good CV statistics at a 20 μM threshold. This is in contrast to the random predictions at 10 μM (Figure S3).

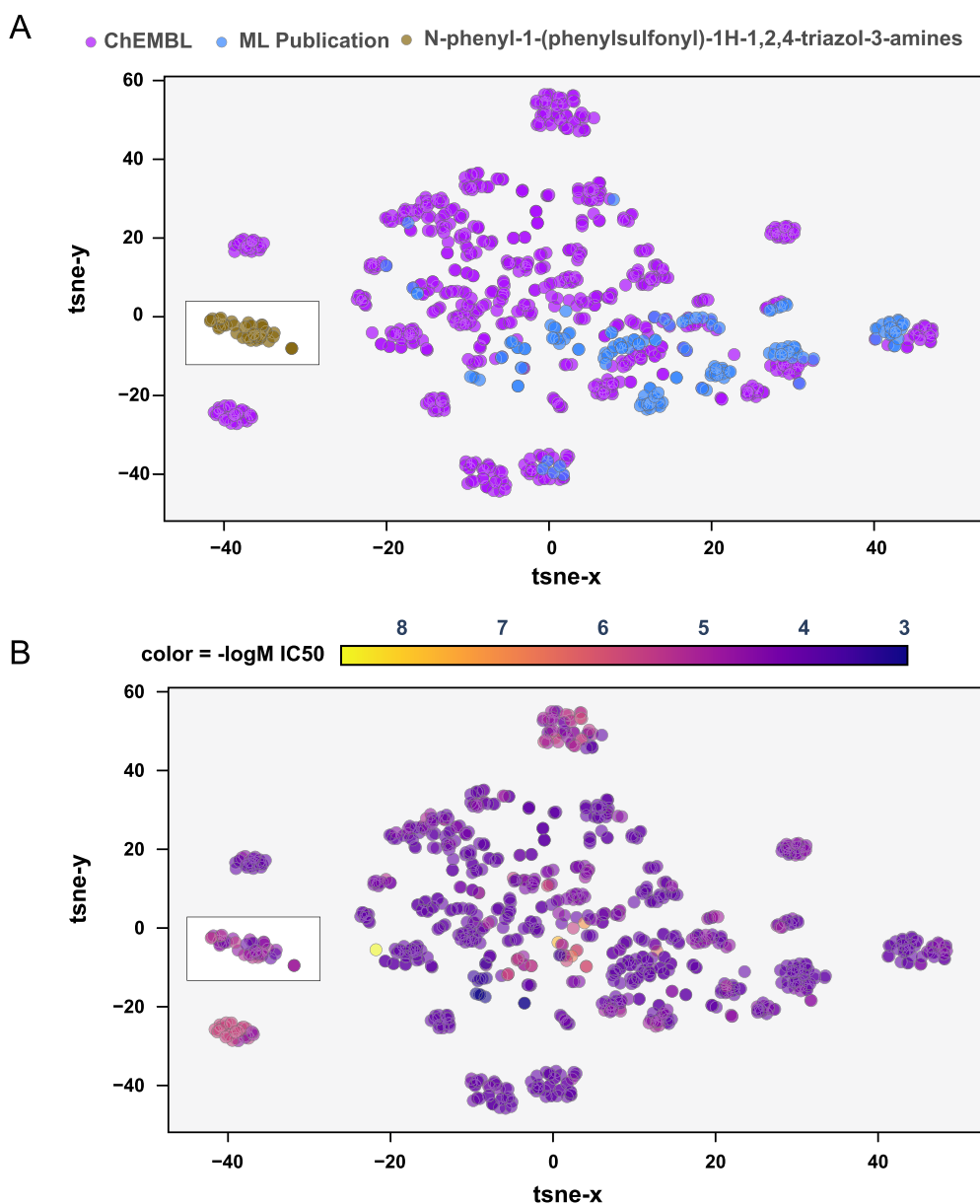


Figure 4. t-SNE visualization of the training and test data for the yellow fever inhibition models using ECFP6 descriptors. Data are colored by either data origin (A) or $-\log M IC_{50}$ activity (B). The defined activity value is irrespective of the qualifier, so many compounds with a low value may represent a compound with no activity (i.e., $>100 \mu M$). The white box highlights the cluster containing the compounds testing in this study. For simplicity, duplicate compounds (found in ref 29 and ChEMBL) are identified as ChEMBL only.

t-SNE visualization using ECFP6 descriptors shows that the compounds tested in this study are distinct from those that have been tested against YFV previously (ChEMBL and the literature²⁹), which suggests a reasonable explanation of why this external test set is predicted so poorly (Figure 4A). In order to help to visualize how the activity magnitude correlated with the chemical property space tested, these data sets were also colored by activity (Figure 4B). This shows that the majority of the most potent compounds are grouped into distinct clusters, which upon inspection were found to be analogues of an initial hit molecule.

To determine if some chemical descriptors may be useful to help distinguish between active and inactive compounds for our compound class, we compared these two groups using several simple chemical descriptors (molecular weight, log P, molecular fraction polar surface area, log D (pH 7.4), and the

number of aromatic rings, hydrogen bond acceptor and donor, rings, and rotatable bonds) using a $20 \mu M$ activity threshold cutoff (Figure 5). The majority of the descriptors did not have a statistically significant difference, although the number of rings was the exception. This exception was also noted in the SAR analysis, where the presence of more aromatic rings was generally more active, particularly in the sulfonyl moiety.

This analysis was extended to the larger, concatenated data set using the same activity threshold cutoff (Figure S4). These comparisons showed statistically significant differences for all of the descriptors assessed, with the largest rank and distribution differences found in MW, PSA, number of rings (aromatic and total), and rotatable bonds. To test for statistically significant differences, comparison tests assumed nonparametric data distributions (Mann–Whitney tests).

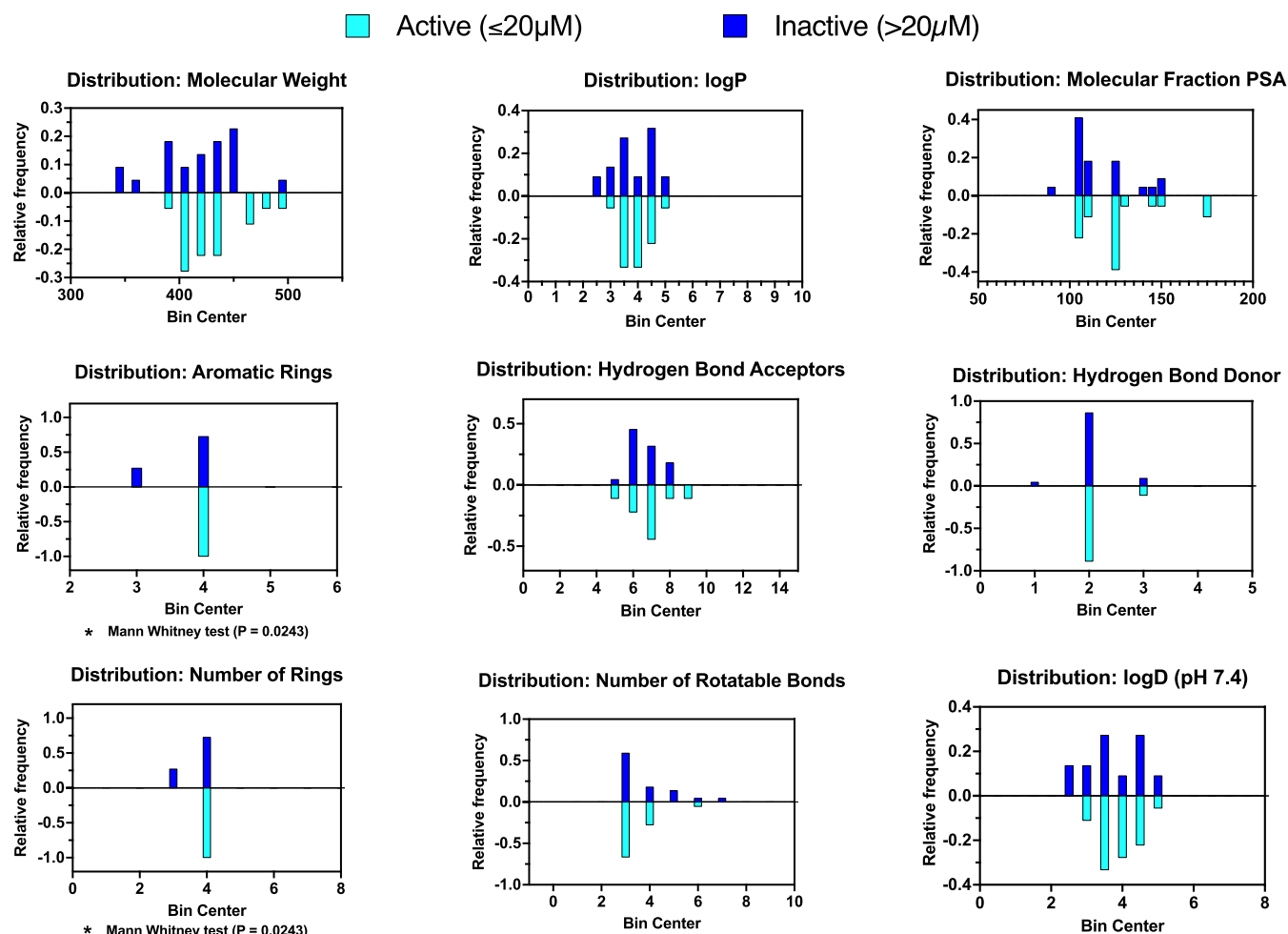


Figure 5. Comparison of simple chemical descriptors between active and inactive classes ($20 \mu\text{M}$ threshold) of the *N*-phenyl-1-(phenylsulfonyl)-1*H*-1,2,4-triazol-3-amines tested. Statistically significant differences, comparison tests assumed nonparametric data distributions (Mann–Whitney tests). Unless noted, differences between groups are not significantly different.

DISCUSSION

As we face new viral pandemics,³⁷ there is a continued need for the identification of broad-spectrum antivirals.³⁸ Many examples of antivirals for YFV have been described that are nucleosides^{39–41} and in contrast, there appear fewer examples of heterocyclic compounds demonstrating activity.^{42,43} We have previously described the identification of the pyrazole-sulfonamide derivative **RCB16003** with low micromolar potency against YFV.²⁹ This represented a starting point for hit-to-lead optimization, which was identified by machine learning. We now describe how this molecule is selective for YF. In an effort to expand our SAR and possibly develop a broader-spectrum molecule, we selected a second class of molecules, which we have been exploring as NNRTI of HIV.³⁵ Compound **RCB16007** had similar *in vitro* activity as the initial hit **RCB16003** but was also found to be active only against West Nile virus as well as YFV. It possessed good *in vitro* ADME properties and excellent mouse PK. **RCB16007** also readily passed the BBB *in vivo*, which may be of importance since there is evidence of YFV BBB penetration.^{44–46} The most substantial evidence of this originates from an outbreak in 2018 in Brazil, where autopsies from 5 of 13 patients that had succumbed to yellow fever showed significant YFV RNA in their CSF.⁴⁶ We explored a further 27 analogues of these two initial hits and were able to improve the *in vitro*

efficacy by 3-fold and the SI 3-fold. We have described our SAR for this series (Figure 2) and propose that **RCB16003**, **RCB16007**, and **RCB17159** may be worth further evaluation for their efficacy against YFV in animal models or lead to the development of further analogues.

We have expanded our earlier machine learning models for YFV to include additional algorithms as well as create further models based on updated data sets. These all showed robust CV scores but failed to be predictive for this new class of compounds. A t-SNE visualization using ECFP6 descriptors showed that the *N*-phenyl-1-(phenylsulfonyl)-1*H*-1,2,4-triazol-3-amines are substantially different from the previously tested compounds, giving a probable reason for the inability of these models to accurately predict the activity of these compounds. While these may not have been useful to predict the activity of these particular compounds, based on the CV score, these could be helpful for the prediction of compounds with more model overlap. Models built with the *N*-phenyl-1-(phenylsulfonyl)-1*H*-1,2,4-triazol-3-amines alone showed mixed CV results, making their use for further optimization ambiguous. Analysis of simple chemical descriptors for the compounds tested against YFV showed the potential importance of the number of rings linked to the activity for this class. Expansion of this analysis included the public data set, where multiple descriptors are suggested to be important for activity. While

these represent multiple classes of compounds, it is interesting that the distribution of actives tended to require an increase in the number of rings over inactives, similar to what we see in the compounds tested in this study. We also found that other simple chemical descriptors showed significant differences between the active and inactive classes, which may be helpful to help predict the activity of novel compounds with activity against YFV in future.

■ ASSOCIATED CONTENT

SI Supporting Information

The Supporting Information is available free of charge at <https://pubs.acs.org/doi/10.1021/acsomega.3c06106>.

General synthesis methods, inhibition assay methods, additional antiviral screening, machine learning models, references, copies of ^1H and ^{13}C NMR spectra, and HPLC traces (PDF)

■ AUTHOR INFORMATION

Corresponding Author

Sean Ekins – Collaborations Pharmaceuticals, Inc., Raleigh, North Carolina 27606, United States; orcid.org/0000-0002-5691-5790; Phone: 215-687-1320; Email: sean@collaborationspharma.com

Authors

Elena Kazakova – Federal Research Centre “Fundamentals of Biotechnology” of the Russian Academy of Sciences (Research Centre of Biotechnology RAS), 119071 Moscow, Russia

Thomas R. Lane – Collaborations Pharmaceuticals, Inc., Raleigh, North Carolina 27606, United States; orcid.org/0000-0001-9240-4763

Thane Jones – Collaborations Pharmaceuticals, Inc., Raleigh, North Carolina 27606, United States; orcid.org/0000-0001-9670-0383

Ana C. Puhl – Collaborations Pharmaceuticals, Inc., Raleigh, North Carolina 27606, United States; orcid.org/0000-0002-1456-8882

Olga Riabova – Federal Research Centre “Fundamentals of Biotechnology” of the Russian Academy of Sciences (Research Centre of Biotechnology RAS), 119071 Moscow, Russia

Vadim Makarov – Federal Research Centre “Fundamentals of Biotechnology” of the Russian Academy of Sciences (Research Centre of Biotechnology RAS), 119071 Moscow, Russia;

orcid.org/0000-0001-8746-2694

Complete contact information is available at:

<https://pubs.acs.org/doi/10.1021/acsomega.3c06106>

Author Contributions

[§]E.K., T.R.L., and T.J. contributed equally to this work. T.R.L. assisted with Assay Central model building and cheminformatics analysis. A.C.P. assisted with compound selection. T.J. assisted with data analysis, interpretation, and SAR. E.K. and O.R. performed molecule synthesis and characterization, and data curation. V.M. and S.E. led the project and designed the experiments. S.E. drafted the initial version of the manuscript. All authors contributed to the manuscript preparation and approved the submitted version of the manuscript.

Notes

The authors declare the following competing financial interest(s): S.E. is owner, A.C.P, T.J. and T.R.L. are employees of Collaborations Pharmaceuticals, Inc. Others have no

competing interests. A provisional patent on this work has been submitted.

■ ACKNOWLEDGMENTS

The authors acknowledge Dr. Mindy Davis, Dr. Amanda Ulloa, and colleagues for assistance with antiviral testing services through NIAID and Dr. Anthony Vocat and Professor Stewart T. Cole for assistance with the *in vitro* evaluation of mutagenicity and cytotoxicity of RCB16007. The authors thank Victor O. Gawriljuk, Dr. Andre S. Godoy, and Dr. Glaucius Oliva for assistance with our earlier efforts on the yellow fever project. Research reported in this publication was supported by the National Institute of Neurological Disorders and Stroke of the National Institutes of Health under Award Number 1R01NS102164-01. The content is solely the responsibility of the authors and does not necessarily represent the official views of the National Institutes of Health. The authors also acknowledge NIH funding R44GM122196-02A1 from NIGMS and 1R43ES031038-01 from NIEHS (PI – Sean Ekins). “Research reported in this publication was supported by the National Institute of Environmental Health Sciences of the National Institutes of Health under Award Number R43ES031038. The content is solely the responsibility of the authors and does not necessarily represent the official views of the National Institutes of Health.” Collaborations Pharmaceuticals, Inc. has utilized the nonclinical and preclinical services program offered by the National Institute of Allergy and Infectious Diseases.

■ ABBREVIATIONS

YFV:yellow fever virus; YF:yellow fever

■ REFERENCES

- (1) Kuno, G.; Chang, G. J.; Tsuchiya, K. R.; Karabatsos, N.; Cropp, C. B. Phylogeny of the genus Flavivirus. *J. Virol* **1998**, *72* (1), 73–83.
- (2) Frierson, J. G. The yellow fever vaccine: a history. *Yale J. Biol. Med.* **2010**, *83* (2), 77–85.
- (3) Gaythorpe, K. A.; Hamlet, A.; Jean, K.; Garkauskas Ramos, D.; Cibrelus, L.; Garske, T.; Ferguson, N., The global burden of yellow fever. *eLife* **2021**, *10*. DOI: 10.7554/eLife.64670.
- (4) Monath, T. P.; Vasconcelos, P. F. Yellow fever. *J. Clin Virol* **2015**, *64*, 160–173.
- (5) Collins, N. D.; Barrett, A. D. Live Attenuated Yellow Fever 17D Vaccine: A Legacy Vaccine Still Controlling Outbreaks In Modern Day. *Curr. Infect Dis. Rep.* **2017**, *19* (3), No. 14.
- (6) Chan, M. Yellow fever: the resurgence of a forgotten disease. *Lancet* **2016**, *387* (10034), 2165–2166.
- (7) Possas, C.; Lourenco-de-Oliveira, R.; Tauil, P. L.; Pinheiro, F. P.; Pissinatti, A.; Cunha, R. V. D.; Freire, M.; Martins, R. M.; Homma, A. Yellow fever outbreak in Brazil: the puzzle of rapid viral spread and challenges for immunisation. *Mem. Inst. Oswaldo Cruz* **2018**, *113* (10), No. e180278.
- (8) Ahmed, Q. A.; Memish, Z. A. Yellow fever from Angola and Congo: a storm gathers. *Trop Doct.* **2017**, *47* (2), 92–96.
- (9) Julander, J. G.; Morrey, J. D.; Blatt, L. M.; Shafer, K.; Sidwell, R. W. Comparison of the inhibitory effects of interferon alfacon-1 and ribavirin on yellow fever virus infection in a hamster model. *Antiviral Res.* **2007**, *73* (2), 140–146.
- (10) de Freitas, C. S.; Higa, L. M.; Sacramento, C. Q.; Ferreira, A. C.; Reis, P. A.; Delvecchio, R.; Monteiro, F. L.; Barbosa-Lima, G.; James Westgarth, H.; Vieira, Y. R.; Mattos, M.; Rocha, N.; Hoelz, L. V. B.; Leme, R. P. P.; Bastos, M. M.; Rodrigues, G. O. L.; Lopes, C. E. M.; Queiroz-Junior, C. M.; Lima, C. X.; Costa, V. V.; Teixeira, M. M.; Bozza, F. A.; Bozza, P. T.; Boechat, N.; Tanuri, A.; Souza, T. M. L.

Yellow fever virus is susceptible to sofosbuvir both in vitro and in vivo. *PLoS Neglected Trop. Dis.* **2019**, *13* (1), No. e0007072.

(11) Julander, J. G.; Bantia, S.; Taubenheim, B. R.; Minning, D. M.; Kotian, P.; Morrey, J. D.; Smeed, D. F.; Sheridan, W. P.; Babu, Y. S. BCX4430, a novel nucleoside analog, effectively treats yellow fever in a Hamster model. *Antimicrob. Agents Chemother.* **2014**, *58* (11), 6607–6614.

(12) Julander, J. G.; Shafer, K.; Smeed, D. F.; Morrey, J. D.; Furuta, Y. Activity of T-705 in a hamster model of yellow fever virus infection in comparison with that of a chemically related compound, T-1106. *Antimicrob. Agents Chemother.* **2009**, *53* (1), 202–209.

(13) Boldescu, V.; Behnam, M. A. M.; Vasilakis, N.; Klein, C. D. Broad-spectrum agents for flaviviral infections: dengue, Zika and beyond. *Nat. Rev. Drug Discovery* **2017**, *16* (8), S65–S86.

(14) DiMasi, J. A.; Grabowski, H. G.; Hansen, R. W. Innovation in the pharmaceutical industry: New estimates of R&D costs. *J. Health Econ.* **2016**, *47*, 20–33.

(15) Macarron, R.; Banks, M. N.; Bojanic, D.; Burns, D. J.; Cirovic, D. A.; Garyantes, T.; Green, D. V.; Hertzberg, R. P.; Janzen, W. P.; Paslay, J. W.; Schopfer, U.; Sittampalam, G. S. Impact of high-throughput screening in biomedical research. *Nat. Rev. Drug Discovery* **2011**, *10* (3), 188–195.

(16) Ganesan, A.; Barakat, K. Applications of computer-aided approaches in the development of hepatitis C antiviral agents. *Expert Opin Drug Discovery* **2017**, *12* (4), 407–425.

(17) Ekins, S.; Freundlich, J. S.; Clark, A. M.; Anantpadma, M.; Davey, R. A.; Madrid, P. Machine learning models identify molecules active against the Ebola virus in vitro. *F1000Res.* **2015**, *4*, 1091.

(18) Ekins, S.; de Siqueira-Neto, J. L.; McCall, L. I.; Sarker, M.; Yadav, M.; Ponder, E. L.; Kallel, E. A.; Kellar, D.; Chen, S.; Arkin, M.; Bunin, B. A.; McKerrow, J. H.; Talcott, C. Machine Learning Models and Pathway Genome Data Base for Trypanosoma cruzi Drug Discovery. *PLoS Neglected Trop. Dis.* **2015**, *9* (6), No. e0003878.

(19) Wicht, K. J.; Combrinck, J. M.; Smith, P. J.; Egan, T. J. Bayesian models trained with HTS data for predicting beta-haematin inhibition and in vitro antimalarial activity. *Bioorg. Med. Chem.* **2015**, *23* (16), 5210–5217.

(20) Weidlich, I. E.; Filippov, I. V.; Brown, J.; Kaushik-Basu, N.; Krishnan, R.; Nicklaus, M. C.; Thorpe, I. F. Inhibitors for the hepatitis C virus RNA polymerase explored by SAR with advanced machine learning methods. *Bioorg. Med. Chem.* **2013**, *21* (11), 3127–3137.

(21) Singh, H.; Singh, S.; Singla, D.; Agarwal, S. M.; Raghava, G. P. QSAR based model for discriminating EGFR inhibitors and non-inhibitors using Random forest. *Biol. Direct* **2015**, *10*, 10.

(22) Franke, L.; Byvatov, E.; Werz, O.; Steinhilber, D.; Schneider, P.; Schneider, G. Extraction and visualization of potential pharmacophore points using support vector machines: application to ligand-based virtual screening for COX-2 inhibitors. *J. Med. Chem.* **2005**, *48* (22), 6997–7004.

(23) Smusz, S.; Kurczab, R.; Satala, G.; Bojarski, A. J. Fingerprint-based consensus virtual screening towards structurally new 5-HT₆R ligands. *Bioorg. Med. Chem. Lett.* **2015**, *25* (9), 1827–1830.

(24) Wei, Y.; Li, J.; Qing, J.; Huang, M.; Wu, M.; Gao, F.; Li, D.; Hong, Z.; Kong, L.; Huang, W.; Lin, J. Discovery of Novel Hepatitis C Virus NSSB Polymerase Inhibitors by Combining Random Forest, Multiple e-Pharmacophore Modeling and Docking. *PLoS One* **2016**, *11* (2), No. e0148181.

(25) Chen, H.; Engkvist, O.; Wang, Y.; Olivecrona, M.; Blaschke, T. The rise of deep learning in drug discovery. *Drug Discovery Today* **2018**, *23* (6), 1241–1250.

(26) Korotcov, A.; Tkachenko, V.; Russo, D. P.; Ekins, S. Comparison of Deep Learning With Multiple Machine Learning Methods and Metrics Using Diverse Drug Discovery Data Sets. *Mol. Pharmaceutics* **2017**, *14* (12), 4462–4475.

(27) Zhavoronkov, A.; Ivanenkov, Y. A.; Aliper, A.; Veselov, M. S.; Aladinskiy, V. A.; Aladinskaya, A. V.; Terentiev, V. A.; Polykovskiy, D. A.; Kuznetsov, M. D.; Asadulaev, A.; Volkov, Y.; Zhulus, A.; Shayakhmetov, R. R.; Zhebrak, A.; Minaeva, L. I.; Zagribelnyy, B. A.; Lee, L. H.; Soll, R.; Madge, D.; Xing, L.; Guo, T.; Aspuru-Guzik,

A. Deep learning enables rapid identification of potent DDR1 kinase inhibitors. *Nat. Biotechnol.* **2019**, *37* (9), 1038–1040.

(28) Rajput, A.; Kumar, M. Anti-flavi: A Web Platform to Predict Inhibitors of Flaviviruses Using QSAR and Peptidomimetic Approaches. *Front. Microbiol.* **2018**, *9*, 3121.

(29) Gawriljuk, V. O.; Foil, D. H.; Puhl, A. C.; Zorn, K. M.; Lane, T. R.; Riabova, O.; Makarov, V.; Godoy, A. S.; Oliva, G.; Ekins, S. Development of Machine Learning Models and the Discovery of a New Antiviral Compound against Yellow Fever Virus. *J. Chem. Inf. Model.* **2021**, *61* (8), 3804–3813.

(30) Vandyck, K.; Rombouts, G.; Stoops, B.; Tahri, A.; Vos, A.; Verschueren, W.; Wu, Y.; Yang, J.; Hou, F.; Huang, B.; Vergauwen, K.; Dehertogh, P.; Berke, J. M.; Raboisson, P. Synthesis and Evaluation of N-Phenyl-3-sulfamoyl-benzamide Derivatives as Capsid Assembly Modulators Inhibiting Hepatitis B Virus (HBV). *J. Med. Chem.* **2018**, *61* (14), 6247–6260.

(31) Kang, D.; Wang, Z.; Chen, M.; Feng, D.; Wu, G.; Zhou, Z.; Jing, L.; Zuo, X.; Jiang, X.; Daelemans, D.; De Clercq, E.; Pannecouque, C.; Zhan, P.; Liu, X. Discovery of potent HIV-1 non-nucleoside reverse transcriptase inhibitors by exploring the structure-activity relationship of solvent-exposed regions I. *Chem. Biol. Drug Des.* **2019**, *93* (4), 430–437.

(32) Lane, T. R.; Urbina, F.; Rank, L.; Gerlach, J.; Riabova, O.; Lepioshkin, A.; Kazakova, E.; Vocat, A.; Tkachenko, V.; Cole, S.; Makarov, V.; Ekins, S. Machine Learning Models for Mycobacterium tuberculosis In Vitro Activity: Prediction and Target Visualization. *Mol. Pharmaceutics* **2022**, *19* (2), 674–689.

(33) Lane, T.; Russo, D. P.; Zorn, K. M.; Clark, A. M.; Korotcov, A.; Tkachenko, V.; Reynolds, R. C.; Perryman, A. L.; Freundlich, J. S.; Ekins, S. Comparing and Validating Machine Learning Models for Mycobacterium tuberculosis Drug Discovery. *Mol. Pharmaceutics* **2018**, *15* (10), 4346–4360.

(34) van der Maaten, L.; Hinton, G. Visualizing Data using t-SNE. *J. Machine Learning Res.* **2008**, *9*, 2579–2605.

(35) Lane, T.; Makarov, V.; Nelson, J. A. E.; Meeker, R. B.; Sanna, G.; Riabova, O.; Kazakova, E.; Monakhova, N.; Tsedilin, A.; Urbina, F.; Jones, T.; Suchy, A.; Ekins, S. N-Phenyl-1-(phenylsulfonyl)-1H-1,2,4-triazol-3-amine as a New Class of HIV-1 Non-nucleoside Reverse Transcriptase Inhibitor. *J. Med. Chem.* **2023**, *66* (9), 6193–6217.

(36) Quillardet, P.; Hofnung, M. The SOS Chromotest, a colorimetric bacterial assay for genotoxins: procedures. *Mutat. Res., Environ. Mutagen. Relat. Subj.* **1985**, *147* (3), 65–78.

(37) Morens, D. M.; Fauci, A. S. Emerging Pandemic Diseases: How We Got to COVID-19. *Cell* **2020**, *183* (3), 837.

(38) Adalja, A.; Inglesby, T. Broad-Spectrum Antiviral Agents: A Crucial Pandemic Tool. *Expert Rev. Anti Infect. Ther.* **2019**, *17* (7), 467–470.

(39) LeCher, J. C.; Zandi, K.; Costa, V. V.; Amblard, F.; Tao, S.; Patel, D.; Lee, S.; da Silva Santos, F. R.; Goncalves, M. R.; Queroz-Junior, C. M.; Marim, F. M.; Musall, K.; Goh, S. L.; McBrayer, T.; Downs-Bowen, J.; De, R.; Azadi, N.; Kohler, J.; Teixeira, M. M.; Schinazi, R. F. Discovery of a 2'-Fluoro,2'-Bromouridine Phosphoramidate Prodrug Exhibiting Anti-Yellow Fever Virus Activity in Culture and in Mice. *Microorganisms* **2022**, *10* (11), 2098 DOI: 10.3390/microorganisms10112098.

(40) De Clercq, E. New Nucleoside Analogues for the Treatment of Hemorrhagic Fever Virus Infections. *Chem. Asian J.* **2019**, *14* (22), 3962–3968.

(41) Lin, K.; Good, S. S.; Julander, J. G.; Weight, A. E.; Moussa, A.; Sommadossi, J. P. AT-752, a double prodrug of a guanosine nucleotide analog, inhibits yellow fever virus in a hamster model. *PLoS Neglected Trop. Dis.* **2022**, *16* (1), No. e0009937.

(42) Gao, Z.; Zhang, X.; Zhang, L.; Wu, S.; Ma, J.; Wang, F.; Zhou, Y.; Dai, X.; Bullitt, E.; Du, Y.; Guo, J. T.; Chang, J. A yellow fever virus NS4B inhibitor not only suppresses viral replication, but also enhances the virus activation of RIG-I-like receptor-mediated innate immune response. *PLoS Pathog.* **2022**, *18* (1), No. e1010271.

(43) Guo, F.; Wu, S.; Julander, J.; Ma, J.; Zhang, X.; Kulp, J.; Cuconati, A.; Block, T. M.; Du, Y.; Guo, J. T.; Chang, J. A Novel Benzodiazepine Compound Inhibits Yellow Fever Virus Infection by Specifically Targeting NS4B Protein. *J. Virol.* **2016**, *90* (23), 10774–10788.

(44) Marinho, P. E. S.; Alvarenga, P. P. M.; Crispim, A. P. C.; Candiani, T. M. S.; Alvarenga, A. M.; Bechler, I. M.; Alves, P. A.; Dornas, F. P.; de Oliveira, D. B.; Bentes, A. A.; Christo, P. P.; Kroon, E. G. Wild-Type Yellow Fever Virus RNA in Cerebrospinal Fluid of Child. *Emerg. Infect. Dis.* **2019**, *25* (8), 1567–1570.

(45) Frassetto, F. P.; Rosemberg, S. Neuropathology of yellow fever autopsy cases. *Trop. Dis. Travel Med. Vaccines* **2023**, *9* (1), No. 1.

(46) Rezende, I. M. d.; Cenachi, A. R. C.; Costa, T. A.; Oliveira, G. F. G.; Rabelo, L.; Menezes, L. M.; Penido, I.; Pereira, L. S.; Arruda, M. S.; Gonçalves, A. P.; Alves, P. A.; Kroon, E. G.; Calzavara-Silva, C. E.; Ramalho, D. B.; Martins-Filho, O. A.; Teixeira-Carvalho, A.; LaBeaud, A. D.; Drumond, B. P. Wild-type Yellow fever virus in cerebrospinal fluid from fatal cases in Brazil, 2018. *Front. Virol.* **2022**, *2*, No. 936191, DOI: 10.3389/fviro.2022.936191.